Multimode gravitational wave detection: the spherical detector theory

José Alberto Lobo

Departament de Física Fonamental
Universitat de Barcelona, Spain
e-mail: lobo@hermes.ffn.ub.es

Abstract

Gravitational waves (GW) are propagated perturbations of the space-time geometry, and they show up locally as *tides*, i.e., local gravity gradients which vary with time. These gradients are determined by *six* often called *electric* components of the Riemann tensor, which in a local coordinate frame are R_{0i0j}, $(i, j = 1, 2, 3)$. A GW detector is a device designed to generate information on those quantities on the basis of suitable measurements. Both Weber bars and laser interferometers are *single mode* antennas, i.e., they generate a *single* readout which is the result of the combined action of those six GW's Riemann tensor amplitudes on the system sensor's output port.

A *spherical* detector is *not* limited in that fashion: this is because its *degenerate* oscillation eigenmodes are uniquely matched to the structure of the above Riemann tensor components. This means that a solid spherical body is a natural *multimode* GW detector, i.e., it is fully capable of delivering six channel outputs, precise combinations of which completely deconvolve the six GW amplitudes.

The present article is concerned with the theoretical reasons of the remarkable properties of a spherical GW detector. The analysis proceeds from *first principles* and is based on essentially no *ad hoc* hypotheses. The mathematical beauty of the theory is outstanding, and abundant detail is given for a thorough understanding of the fundamental facts and ideas. Experimental evidence of the accuracy of the model is also provided, where possible.

Summary

The following pages contain the fusion of two published papers: *What can we learn about gravitational wave physics with an elastic spherical antenna?*, published in the *Physical Review* (PRD **52**, 591-604 (1995)), and *Multiple mode gravitational wave detection with a spherical antenna*, scheduled to appear in the July-2000 issue of *Monthly Notices of the Royal Astronomical Society* (MNRAS **316**, 173-194 (2000))[1]. In them, I first developed an analytic model to describe the interaction of a solid elastic sphere with an incoming flux of gravitational waves of the general *metric* class, then extended it to also address the multimode signal deconvolution problem by means of suitable layouts of *resonant* motion sensors.

I think the model is quite complete as regards the major *conceptual* issues in a spherical GW detector, therefore think merging the two papers together makes positive sense. Let me however stress that I do not mean to understate the fundamental problem of *noise*, which is here left aside; rather, it is now being actively investigated in detail within the very convenient general framework set up below.

What can we learn about GW Physics . . . is already five years old, and certain parts of it have been the subject of further research since. More specifically, this happens with Brans-Dicke absorption cross sections, see section 4, where reference has been added to such newer work. In addition, two new tables and more mathematical detail have been added to its Appendix B. The latter should help the interested reader with certain technicalities, while the tables and attendant new formulas are meant to provide explicit numerical values of the frequency spectrum of the sphere rather than the original *only graphics* information. I expect this to be useful reference in numerical and/or experimental determinations of these quantities.

No changes have been included in the second paper relative to its MNRAS version. In merging the two articles together, however, I have found expedient to renumber the equations and bibliographic references into corresponding single streams. The bibliography has been updated and made into a unique list at the end of the file in alphabetical order. Finally, I have included minor notation changes in order to reconcile otherwise small mistunings between both articles.

Alberto Lobo
Barcelona, June 2000

[1] The research contained in this second paper was actually complete by early 1996, and its main results first presented in a Winter School at Warsaw (Poland) in march 1996 [39], then in a plenary lecture at the *Second Edoardo Amaldi Conference on Gravitational Waves* at *CERN* in July 1997 [41]. Essentially in its present form —see acknowledgements in page 48 below—, the paper was submitted to PRD in 1997. It was rejected *after* the Editor, Dennis Nordstrom, had already accepted it, on the basis of a positive report. The reason for this opinion switch was a later, extremely vague yet demolishingly negative and utterly arrogant judgement by a second referee, to whom Nordstrom grants unlimited credit.

An *unchanged* version of the manuscript was, again, positively reported on for MNRAS, and so the article will at long last see the light, three years too late.

What can we learn about GW Physics with an elastic spherical antenna?

PRD **52**, 591-604 (1995)

José Alberto Lobo

Departament de Física Fonamental
Universitat de Barcelona, Spain
e-mail: lobo@hermes.ffn.ub.es

Abstract

A general formalism is set up to analyse the response of an *arbitrary* solid elastic body to an *arbitrary metric* Gravitational Wave perturbation, which fully displays the details of the interaction wave-antenna. The formalism is applied to the spherical detector, whose sensitivity parameters are thereby scrutinised. A *multimode* transfer function is defined to study the amplitude sensitivity, and absorption cross sections are calculated for a general metric theory of GW physics. Their *scaling* properties are shown to be *independent* of the underlying theory, with interesting consequences for future detector design. The GW incidence direction deconvolution problem is also discussed, always within the context of a general metric theory of the gravitational field.

1 Introduction

Spherical antennae are considered by many to be the natural next step in the development of resonant GW detectors. The reasons for this new trend essentially derive from the *improved sensitivity* of a sphere —which can be nearly an order of magnitude better than a cylinder having the same resonance frequency, see below and [13]—, and from its *multimode capabilities*, first recognised by Forward [22] and further elaborated in [61, 30].

Although some of the most relevant aspects of detector sensitivity have already received attention in the literature, it seems to me that a sufficiently general and flexible analysis of the interaction between GW and detector has not been satisfactorily developed to date. This *theoretical* shortage has a number of *practical* negative consequences, too. Traditional analysis, to mention but an example, is almost invariably restricted to General Relativity or scalar–tensor theories of gravity; while it may be argued that this is already very general, any such argument is, as a matter of fact, understating the potentialities actually offered by a spherical GW antenna to help decide for or against any one specific theory of the gravitational field on the basis of *experimental observation*.

I thus propose to develop in this paper a full fledged mathematical formalism which will enable analysis of the antenna's response to a completely general GW, i.e., making no *a priori* assumptions about which is the correct theory underlying GW physics (other than, indeed, that it is a *metric* theory), *and* also making no assumptions about detector shape, structure or boundary conditions. Considering things in such generality is not only "theoretically nice" —it also brings about new results and a *better understanding* of older ones. For example, it will be proved that the sphere is the *most efficient* GW elastic detector shape, and that higher mode absorption cross sections *scale independently of GW physics*. I will also discuss the direction of incidence deconvolution problem in the context of a general metric theory of gravity.

The paper is organised as follows: section 2 is devoted to the development of the general mathematical framework, leading to a formula in which an elastic solid's response is related to the action of an arbitrary metric GW impinging on it. In section 3 the general equations are applied to the homogeneous spherical body, and a discussion of the *deconvolution* problem is presented as well. Section 4 contains the description of the sphere's sensitivity parameters, specifically leading to the concept of

multimode, or vector, *transfer function*, and to an analysis of the *absorption cross section* presented by this detector to a passing by GW. Conclusions and prospects are summarised in section 5, and two appendices are added which include mathematical derivations.

2 General mathematical framework

In the mathematical model, I shall be assuming that the antenna is a solid elastic body which responds to GW perturbations according to the equations of classical non-relativistic linear Elasticity Theory [32]. This is fully justified because GW-induced displacements will be very small indeed, and the speed of such displacements much smaller than that of light for any foreseeable frequencies. Although our primary interest is a spherical antenna, the considerations which follow in the remainder of this section *have general validity for arbitrarily shaped, isotropic elastic solids*.

Let $\mathbf{u}(\mathbf{x},t)$ be the displacement vector of the infinitesimal mass element sitting at point $\mathbf{x}$ relative to the solid's centre of mass in its unperturbed state, whose density distribution in that state is ϱ. Let λ and μ be the material's elastic Lamé coefficients. If a volume force density $\mathbf{f}(\mathbf{x},t)$ acts on such solid, the displacement field $\mathbf{u}(\mathbf{x},t)$ is the solution to the system of partial differential equations [32]

$$\varrho\frac{\partial^2\mathbf{u}}{\partial t^2}-\mu\nabla^2\mathbf{u}-(\lambda+\mu)\,\nabla(\nabla\cdot\mathbf{u})=\mathbf{f}(\mathbf{x},t) \tag{1}$$

with the appropriate initial and boundary conditions. A summary of notation and general results regarding the solution to that system is briefly outlined in the ensuing subsection, as they are necessary for the subsequent developments in this paper, and also in future work —e.g. page 25 and ss. below.

2.1 Separable driving force

For reasons which will become clear later on, we shall only be interested in driving forces of the separable type

$$\mathbf{f}(\mathbf{x},t)=\mathbf{f}(\mathbf{x})\,g(t) \tag{2}$$

or, indeed, linear combinations thereof. The solution to (1) does not require us to specify the precise boundary conditions on $\mathbf{u}(\mathbf{x},t)$ at this stage, but we need to set the initial conditions. We adopt the following:

$$\mathbf{u}(\mathbf{x},0)=\dot{\mathbf{u}}(\mathbf{x},0)=0 \tag{3}$$

where $\dot{}\equiv\partial/\partial t$, implying that the antenna is at complete rest before observation begins at t=0. The structure of the force field (2) is such that the displacements $\mathbf{u}(\mathbf{x},t)$ can be expressed by means of a *Green function* integral of the form

$$\mathbf{u}(\mathbf{x},t)=\int_0^\infty \mathbf{S}(\mathbf{x};t-t')\,g(t')\,dt' \tag{4}$$

The deductive procedure whereby $\mathbf{S}(\mathbf{x};t-t')$ is calculated can be found in many standard textbooks —see e.g. [60]. The result is

$$\mathbf{S}(\mathbf{x};t)=\begin{cases}0 & \text{if}\quad t\le 0\\ \sum_N \frac{f_N}{\omega_N}\,\mathbf{u}_N(\mathbf{x})\sin\omega_N t & \text{if}\quad t\ge 0\end{cases} \tag{5}$$

where

$$f_N\equiv\frac{1}{M}\int_{\text{Solid}}\mathbf{u}_N^*(\mathbf{x})\cdot\mathbf{f}(\mathbf{x})\,d^3x \tag{6}$$

and $\mathbf{u}_N(\mathbf{x})$ are the normalised *eigen–solutions* to

$$\mu\nabla^2\mathbf{u}_N + (\lambda+\mu)\,\nabla(\nabla\cdot\mathbf{u}_N) = -\omega_N^2\varrho\mathbf{u}_N \tag{7}$$

with suitable *boundary conditions*. Here N represents an index, or set of indices, labelling the *eigenmode* of frequency ω_N. The normalisation condition is (arbitrarily) chosen so that

$$\int_{\text{Solid}} \mathbf{u}^*_{N'}(\mathbf{x})\cdot\mathbf{u}_N(\mathbf{x})\,\varrho(\mathbf{x})\,d^3x = M\,\delta_{N'N} \tag{8}$$

where M is the total mass of the solid, and the asterisk denotes complex conjugation. Replacing now (5) into (4) we can write the solution to our problem as a series expansion:

$$\mathbf{u}(\mathbf{x},t) = \sum_N \frac{f_N}{\omega_N}\,\mathbf{u}_N(\mathbf{x})\,g_N(t) \tag{9}$$

where

$$g_N(t) \equiv \int_0^t g(t')\,\sin\omega_N(t-t')\,dt' \tag{10}$$

Equation (9) is the *formal* solution to our problem; it has the standard form of an orthogonal expansion and is valid for *any* solid driven by a separable force like (2) and *any* boundary conditions. It is therefore *completely general*, given that type of force.

Before we go on, it is perhaps interesting to quote a simple but useful example. It is the case of a solid hit by a *hammer blow*, i.e., receiving a sudden stroke at a point on its surface. Exam of the response of a GW antenna to such perturbation is being used for correct tuning and monitoring of the device [29]. If the driving force density is represented by the simple model

$$\mathbf{f}^{(\text{hb})}(\mathbf{x},t) = \mathbf{f}_0\,\delta^{(3)}(\mathbf{x}-\mathbf{x}_0)\,\delta(t) \tag{11}$$

where $\mathbf{x}_0$ is the surface point hit, and $\mathbf{f}_0$ is a constant vector, then the system's response is immediately seen to be

$$\mathbf{u}^{(\text{hb})}(\mathbf{x},t) = \sum_N \frac{f^0_N}{\omega_N}\,\mathbf{u}_N(\mathbf{x})\sin\omega_N t \tag{12}$$

with $f^0_N = M^{-1}\,\mathbf{f}_0\cdot\mathbf{u}^*_N(\mathbf{x}_0)$. A hammer blow thus excites *all* the solid's normal modes, except those *perpendicular* to $\mathbf{f}_0$, with amplitudes which are *inversely proportional to the mode's frequency*. This is seen to be a rather general result in the theory of sound waves in isotropic elastic solids.

2.2 The GW tidal forces

An incoming GW manifests itself as a *tidal* force density; in the long wavelength linear approximation [54] it only depends on the "electric" components of the Riemann tensor:

$$f_i(\mathbf{x},t) = \varrho c^2\,R_{0i0j}(t)\,x_j \tag{13}$$

where c is the speed of light, and sum over the repeated index j is understood. In (13) tidal forces are referred to the antenna's centre of mass, and thus $\mathbf{x}$ is a vector originating there. Note that I have omitted any dependence of R_{0i0j} on spatial coordinates, since it only needs to be evaluated at the solid's centre. The Riemann tensor is only required to first order at this stage [62]:

$$R_{0i0j} = \frac{1}{2}\,(h_{ij,00} - h_{0i,0j} - h_{0j,0i} + h_{00,ij}) \tag{14}$$

where $h_{\mu\nu}$ are the perturbations to flat geometry[2], always at the centre of mass of the detector.

The form (13) is seen to be a sum of three terms like (2) —but this three term "straightforward" splitting is not the most convenient, due to lack of invariance and symmetry. A better choice is now outlined.

An *arbitrary symmetric* tensor $\mathcal{S}_{ij}$ admits the following decomposition:

$$\mathcal{S}_{ij}(t) = \mathcal{S}^{(00)}(t)\, E^{(00)}_{ij} \;+\; \sum_{m=-2}^{2} \mathcal{S}^{(2m)}(t)\, E^{(2m)}_{ij} \tag{15}$$

where $E^{(2m)}_{ij}$ are 5 linearly independent *symmetric* and *traceless* tensors, and $E^{00)}_{ij}$ is a multiple of the *unit* tensor δ_{ij}. $\mathcal{S}^{(lm)}(t)$ are uniquely defined functions, whose explicit form depends on the particular representation of the E-matrices chosen. A convenient one is the following:

$$E^{(00)}_{ij} = \left(\tfrac{1}{4\pi}\right)^{\frac{1}{2}} \begin{pmatrix} 1 & 0 & 0 \\ 0 & 1 & 0 \\ 0 & 0 & 1 \end{pmatrix} \tag{16.a}$$

$$E^{(20)}_{ij} = \left(\tfrac{5}{16\pi}\right)^{\frac{1}{2}} \begin{pmatrix} -1 & 0 & 0 \\ 0 & -1 & 0 \\ 0 & 0 & 2 \end{pmatrix} \;,\quad E^{(2\pm1)}_{ij} = \left(\tfrac{15}{32\pi}\right)^{\frac{1}{2}} \begin{pmatrix} 0 & 0 & \mp 1 \\ 0 & 0 & -i \\ \mp 1 & -i & 0 \end{pmatrix} \tag{16.b}$$

$$E^{(2\pm2)}_{ij} = \left(\tfrac{15}{32\pi}\right)^{\frac{1}{2}} \begin{pmatrix} 1 & \pm i & 0 \\ \pm i & -1 & 0 \\ 0 & 0 & 0 \end{pmatrix} \tag{16.c}$$

The excellence of this representation stems from its ability to display the *spin features* of the driving terms in (13). Such features are characterised by the relationships

$$E^{(lm)}_{ij}\, n_i n_j = Y_{lm}(\mathbf{n}) \;, \qquad l = 0, 2 \;; \qquad m = -l, \ldots, l \tag{17}$$

where $\mathbf{n} \equiv \mathbf{x}/|\mathbf{x}|$ is the radial unit vector, and $Y_{lm}(\mathbf{n})$ are spherical harmonics [21]. Details about the above E-matrices are given in Appendix A. In particular, the orthogonality relations (55) can be used to invert (15):

$$\mathcal{S}^{(00)}(t) \;=\; \frac{4\pi}{3}\, E^{(00)}_{ij}\, \mathcal{S}_{ij}(t) \tag{18.a}$$

$$\mathcal{S}^{(2m)}(t) \;=\; \frac{8\pi}{15}\, E^{*(2m)}_{ij}\, \mathcal{S}_{ij}(t) \;, \qquad m = -2, \ldots, 2 \tag{18.b}$$

where an asterisk denotes complex conjugation. Note that $\mathcal{S}^{(00)}(t) = \sqrt{4\pi}\mathcal{S}(t)/3$, where $\mathcal{S}(t) \equiv \delta_{ij}\, \mathcal{S}_{ij}(t)$ is the tensor's trace.

We now take advantage of (15) to express the GW tidal force (13) as a sum of split terms like (2):

$$\mathbf{f}(\mathbf{x}, t) = \mathbf{f}^{(00)}(\mathbf{x})\, g^{(00)}(t) \;+\; \sum_{m=-2}^{2} \mathbf{f}^{(2m)}(\mathbf{x})\, g^{(2m)}(t) \tag{19}$$

with

[2] Throughout this paper, *Greek* indices $(\mu, \nu, \ldots)$ will run through space-time values 0,1,2,3; *Latin* indices $(i, j, \ldots)$ will run through space values 1,2,3 only.

$$f_i^{(00)}(\mathbf{x}) = \varrho\, E_{ij}^{(00)}\, x_j \qquad , \qquad g^{(00)}(t) = \frac{4\pi}{3}\, E_{ij}^{*(00)}\, R_{0i0j}(t)\, c^2 \tag{20.a}$$

$$f_i^{(2m)}(\mathbf{x}) = \varrho\, E_{ij}^{(2m)}\, x_j \qquad , \qquad g^{(2m)}(t) = \frac{8\pi}{15}\, E_{ij}^{*(2m)}\, R_{0i0j}(t)\, c^2 \qquad (m = -2, \ldots, 2) \tag{20.b}$$

Straightforward application of (9) yields the formal solution of the antenna response to a GW perturbation:

$$\mathbf{u}(\mathbf{x}, t) = \sum_N \omega_N^{-1} \mathbf{u}_N(\mathbf{x}) \left[f_N^{(00)}\, g_N^{(00)}(t) \; + \; \sum_{m=-2}^{2} f_N^{(2m)}\, g_N^{(2m)}(t) \right] \tag{21}$$

with the notation of (6) and (10) applied *mutatis mutandi* to the terms in (20).

Equation (21) gives the response of an arbitrary elastic solid to an incoming weak GW, *independently of the underlying gravity theory*, be it General Relativity (GR) or indeed any other *metric* theory of the gravitational interaction. It is also valid for *any antenna shape* and *any boundary conditions*, thus giving the formalism, in particular, the capability of being used to study the response of a detector which is *suspended* by means of a mechanical device in the laboratory site —a situation of much practical importance. It is therefore *very* general.

Equation (21) also tells us that that only *monopole* and *quadrupole detector modes* can possibly be excited by a metric GW. The nice thing about (21) is that it *fully* displays the monopole-quadrupole *structure* of the solution to the fundamental differential equations (1).

In a non-symmetric body, all (or *nearly* all) the modes have monopole and quadrupole moments, and (21) precisely shows how much each of them contributes to the detector's response. A *homogeneous spherical* antenna, which is very symmetric, has a set of vibrational eigenmodes which are particularly well matched to the form (21): it only possesses *one* series of monopole modes and *one* (five-fold degenerate) series of quadrupole modes —see next section and Appendix B for details. The existence of so *few* modes which couple to GWs means that *all the absorbed incoming radiation energy will be distributed amongst those few modes only*, thereby making the sphere the *most efficient* detector, even from the sensitivity point of view. The higher energy cross section *per unit mass* reported for spheres on the basis of GR [13], for example, finds here its qualitative explanation. The generality of (21), on the other hand, means that *this excellence of the spherical detector is there independently of which is the correct GW theory.*

Before going further, let me mention another potentially useful application of the formalism so far. Cylindrical antennas, for instance, are usually studied in the *thin rod* approximation; although this is generally quite satisfactory, equation (21) offers the possibility of eventually considering corrections to such simplifying hypothesis by use of more realistic eigenfunctions, such as those given in [27, 56]. Recent new proposals for stumpy cylinder arrays [8] may well benefit from the above approach, too.

3 The spherical antenna

To explore the consequences of (21) in a particular case, the mode amplitudes $\mathbf{u}_N(\mathbf{x})$ and frequencies ω_N must be specified. From now on I will focus on a *homogeneous sphere* whose surface is free of tractions and/or tensions; the latter happens to be quite a good approximation, even if the sphere is suspended in the static gravitational field [34].

The normal modes of the free sphere fall into two families: so called *toroidal* —where the sphere only undergoes twisting which keep its shape unchanged throughout the volume— and *spheroidal* [35], where radial as well as tangential displacements take place. I use the notation

$$\mathbf{u}_{nlm}^T(\mathbf{x})\, e^{\pm i\omega_{nl}^T t} \qquad , \qquad \mathbf{u}_{nlm}^P(\mathbf{x})\, e^{\pm i\omega_{nl}^P t} \tag{22}$$

for them, respectively; note that the index N of the previous section is a *multiple* index $\{nlm\}$ for *each* family; l and m are the usual *multipole* indices, and n numbers from 1 to ∞ each of the l-pole modes. The frequencies happen to be independent of m, and so every one mode (22) is $(2l+1)$-fold degenerate. Further details about these eigenmodes are given in Appendix B.

In order to see what (21) looks like in this case, integrals of the form (6) ought to be evaluated. It is straightforward to prove that they all vanish for the toroidal modes, the spheroidal modes contributing the only non-vanishing terms; after some algebra one finds

$$f^{(l'm')}_{nlm} \equiv \frac{1}{M}\int_{\rm Sphere} \mathbf{u}^{P\,*}_{nlm}(\mathbf{x})\cdot\mathbf{f}^{(l'm')}(\mathbf{x})\,d^3x = a_{nl}\,\delta_{l'l}\,\delta_{m'm}\ , \qquad l'=0,2,\ m'=-l',\ldots,l' \tag{23}$$

where

$$a_{n0} \;=\; -\frac{1}{M}\int_0^R A_{n0}(r)\,\varrho\,r^3\,dr \tag{24.a}$$

$$a_{n2} \;=\; -\frac{1}{M}\int_0^R \left[A_{n2}(r)+3\,B_{n2}(r)\right]\,\varrho\,r^3\,dr \tag{24.b}$$

The functions $A_{nl}(r)$, $B_{nl}(r)$ are given in Appendix B, and R is the sphere's radius. To our reassurance, only the monopole and quadrupole *sphere modes* survive, as seen by the presence of the factors $\delta_{l'l}$ in (23). The final series is thus a relatively simple one, even in spite of its generality[3]:

$$\mathbf{u}(\mathbf{x},t) = \sum_{n=1}^{\infty}\frac{a_{n0}}{\omega_{n0}}\,\mathbf{u}_{n00}(\mathbf{x})\,g^{(00)}_{n0}(t)\ +\ \sum_{n=1}^{\infty}\frac{a_{n2}}{\omega_{n2}}\left[\sum_{m=-2}^{2}\mathbf{u}_{n2m}(\mathbf{x})\,g^{(2m)}_{n2}(t)\right]\ , \qquad (t>0) \tag{25}$$

where, it is recalled,

$$g^{(lm)}_{nl}(t) = \int_0^t g^{(lm)}(t')\,\sin\omega_{nl}(t-t')\,dt'\ , \qquad (l=0,2;\quad m=-l,\ldots,l) \tag{26}$$

Equation (25) constitutes the sphere's response to an arbitrary tidal GW perturbation, and will be used to analyse the sensitivity of the spherical detector in the next section. Before doing so, however, a few comments on the antenna's signal *deconvolution capabilities*, within the context of a completely general metric theory of GWs, are in order.

3.1 The deconvolution problem

Let us first of all take the Fourier transform of (25):

$$\mathbf{U}(\mathbf{x},\omega) \equiv \int_{-\infty}^{\infty}\mathbf{u}(\mathbf{x},t)\,e^{-i\omega t}\,dt \tag{27}$$

This is seen to be

$$\begin{aligned}\mathbf{U}(\mathbf{x},\omega) \;&=\; \frac{\pi}{i}\sum_{n=1}^{\infty}\frac{a_{n0}}{\omega_{n0}}\,\mathbf{u}_{n00}(\mathbf{x})\,G^{(00)}(\omega)\left[\delta(\omega-\omega_{n0})-\delta(\omega+\omega_{n0})\right]\ +\\ &+\ \frac{\pi}{i}\sum_{n=1}^{\infty}\frac{a_{n2}}{\omega_{n2}}\left[\sum_{m=-2}^{2}\mathbf{u}_{n2m}(\mathbf{x})\,G^{(2m)}(\omega)\right]\left[\delta(\omega-\omega_{n2})-\delta(\omega+\omega_{n2})\right]\end{aligned} \tag{28}$$

[3] From now on I will drop the label P, meaning *spheroidal* mode, to ease the notation since *toroidal* modes no longer appear in the formulae.

where $G^{(lm)}(\omega)$ are the Fourier transforms of $g^{(lm)}(t)$, respectively:

$$G^{(lm)}(\omega) \equiv \int_0^\infty g^{(lm)}(t)\, e^{-i\omega t}\, dt \tag{29}$$

The δ-function factors are of course idealisations corresponding to infinitely long integration times and infinitely narrow resonance line-widths —but the essentials of the ensuing discussion will not be affected by those idealisations.

If the measuring system were (ideally) sensitive to all frequencies, filters could be applied to examine the antenna's oscillations at each monopole and quadrupole frequency: a single transducer would suffice to reveal $G^{(00)}(\omega)$ around the monopole frequencies ω_{n0}, whilst *five* (placed at suitable positions) would be required to calculate the five degenerate amplitudes $G^{(2m)}(\omega)$ around the quadrupole frequencies ω_{n2}. Once the *six* functions $G^{(lm)}(\omega)$ would have thus been determined, inverse Fourier transforms would give us the functions $g^{(lm)}(t)$, and thereby the six Riemann tensor components $R_{0i0j}(t)$ through inversion of the second of equations (20), i.e., as an expansion like (15) —only with g's instead of $\mathcal{S}$'s. Deconvolution would then be complete.

Well, not quite... Knowledge of the Riemann tensor in the *laboratory* frame coordinates is not really sufficient to say the waveform has been completely deconvolved, unless we *also* know the *source position* in the sky. There clearly are two possibilities:

i) The source position *is* known ahead of time by some other astronomical observation methods. Let me rush to emphasise that, far from trivial or uninteresting, this is a *very important* case to consider, specially during the first stages of GW Astronomy, when any reported GW event will have to be thoroughly checked by all possible means.

   If the incidence direction is known, then a rotation must be applied to the just obtained quantities $R_{0i0j}(t)$, which takes the laboratory z-axis into coincidence with the incoming wave propagation vector. A classification procedure must thereafter be applied to the so transformed Riemann tensor in order to see which is the theory (or class of theories) compatible with the actual observations. Such classification procedure has been described in detail in [20]; see also [49] for an updated discussion.

   The spherical antenna is thus seen to have the *capability of furnishing the analyst sufficient information to discern amongst different competing theories of GW physics, whenever the wave incidence direction is known prior to detection.*

ii) The source position is *not* known at detection time. This makes things more complex, since the above rotation between the laboratory and GW frames cannot be performed.

   In order to deconvolve the incidence direction in this case, a specific theory of the GWs *must* be assumed —a given choice being made on the basis of whatever prior information is available or, simply, dictated by the the decision to probe a particular theory. Wagoner and Paik [61] propose a method which is useful both for GR and BD theory, their idea being simple and elegant at the same time: since neither of these theories predicts the excitation of the $m{=}\pm1$ quadrupole modes *of the wave*, the source position is determined precisely by the rotation angles which, when applied to the laboratory axes, cause the amplitudes of those *antenna* modes to vanish; the rotated frame is thereby associated to the GW natural frame.

   A generalisation of this idea can conceivably be found on the basis of a detailed —and possibly rather casuistic— analysis of the canonical forms of of the Riemann tensor for a list of theories of gravity, along the following line of argument: any one particular theory will be characterised by certain (homogeneous) canonical relationships amongst the monopole and quadrupole components of the Riemann tensor, $g^{(lm)}(t)$, and so enforcement of those relations upon rotation of the laboratory frame axes should enable determination of the rotation angles or, equivalently, of

the incoming radiation incidence direction. Scalar-tensor theories e.g. have $g^{(2\pm1)}(t) = 0$ in their canonical forms, hence Wagoner and Paik's proposal for this particular case.

Before any deconvolution procedure is triggered, however, it is very important to make sure that it will be *viable*. More precisely, since the transformation from the laboratory to the ultimate canonical frame is going to be linear, *invariants* must be preserved. This means that, even if the source position is unknown, certain theories will forthrightly be *vetoed* by the observed $R_{0i0j}(t)$ if their predicted invariants are incompatible with the observed ones. To give but an easy example, if $R_{0i0j}(t)$ is *observed* to have a non-null trace $R_{0i0i}(t)$, then a veto on GR will be readily served, and therefore no algorithm based on that theory should be applied [51].

I would like to make a final remark here. Assume a direction deconvolution procedure has been successfully carried through to the end on the basis of certain GW theory, so that the analyst comes up with a pair of numbers (θ, φ) expressing the source's coordinates in the sky. Of course, these numbers will represent the *actual* source position *only if the assumed theory is correct*. Now, how do we know it *is* correct? Strictly speaking, "correctness" of a scientific theory is an *asymptotic* concept —in the sense that the possibility always remains open that new facts be eventually discovered which contradict the theory—, and so *reliability* of the estimate (θ, φ) of the source position can only be assessed in practice in terms of the *consistency* between the assumed theory and whatever experimental evidence is available *to date*, including, indeed, GW measurements themselves. It is thus very important to have a method to verify that the estimate (θ, φ) does not contradict the theory which enabled its very determination.

Such verification is a *logical* absurdity if only *one* measurement of position is available; this happens for instance if the recorded signal is a *short burst* of radiation, and so *two antennas* are at least necessary to check consistency in that case. The test would proceed as a check that the time delay between reception of the signal at both detectors is consistent with the calculated (θ, φ)[4], given their relative position and the wave propagation speed predicted by the assumed theory. If, on the other hand, the signal being tracked is a *long duration* signal, then a single antenna may be sufficient to perform the test by looking at the observed Doppler patterns and checking them against those expected with the given (θ, φ).

The above considerations have been made ignoring noise in the detector and monitor systems. A fundamental constraint introduced by noise is that it makes the antenna *bandwidth limited* in sensitivity. As a consequence, any deconvolution procedure is deemed to be incomplete or, rather, *ambiguous* [5], since information about the signal can possibly be retrieved only within a reduced bandwidth, whilst the rest will be lost. I thus come to a detailed discussion of the sensitivity of the spherical GW antenna in the next section.

4 The sensitivity parameters

I will consider successively *amplitude* and *energy* sensitivities; the first leads to the concept of *transfer function*, while the second to that of absorption *cross section*. I devote separate subsections to analyse each of them in some detail.

4.1 The transfer function

A widely used and useful concept in linear system theory is that of *transfer function* [26]. It is defined as the Fourier transform of the system's impulse response, or as the system's impedance/admittance, and can be inferred from the frequency response function (28).

[4] Note that the two detectors will agree on the same (θ, φ), even if the assumed theory is wrong, since the sphere deformations will be the same if caused by the same signal.

We recall from the previous section that the sphere is a multimode device —due to its monopole and five-fold degenerate quadrupole modes. It is expedient to define a *multimode* or *vector transfer function* as a useful construct which encompasses all six different modes into a single conceptual block, according to

$$\mathbf{U}(\mathbf{x},\omega) = \sum_{\alpha} \mathbf{Z}^{(\alpha)}(\mathbf{x},\omega)\, G^{(\alpha)}(\omega) \tag{30}$$

where $G^{(\alpha)}(\omega)$ are the six driving terms $G^{(lm)}(\omega)$ given in (29). The transfer function is $\mathbf{Z}^{(\alpha)}(\mathbf{x},\omega)$, and its "vector" character alluded above is reflected by the *multimode index* α. Looking at (28) it is readily seen that

$$\mathbf{Z}^{(00)}(\mathbf{x},\omega) \;=\; \frac{\pi}{i}\sum_{n=1}^{\infty} \frac{a_{n0}}{\omega_{n0}}\,\mathbf{u}_{n00}(\mathbf{x})\;[\delta(\omega-\omega_{n0}) - \delta(\omega+\omega_{n0})] \tag{31.a}$$

$$\mathbf{Z}^{(2m)}(\mathbf{x},\omega) \;=\; \frac{\pi}{i}\sum_{n=1}^{\infty} \frac{a_{n2}}{\omega_{n2}}\,\mathbf{u}_{n2m}(\mathbf{x})\;[\delta(\omega-\omega_{n2}) - \delta(\omega+\omega_{n2})] \qquad (m=-2,\ldots,2) \tag{31.b}$$

As we observe in these formulae, the sphere's sensitivity to monopole excitations is governed by a_{n0}/ω_{n0}, and to quadrupole ones by a_{n2}/ω_{n2}. Closed expressions happen to exist for a_{n0} and a_{n2}; using the notation of Appendix B, they are

$$\frac{a_{n0}}{R} \;=\; \frac{3\,C(n,0)}{8\pi}\;\frac{j_2(q_{n0}R)}{q_{n0}R} \tag{32.a}$$

$$\frac{a_{n2}}{R} \;=\; -\frac{3\,C(n,2)}{8\pi}\left[\beta_3(k_{n2}R)\,\frac{j_2(q_{n2}R)}{q_{n2}R} - 3\,\frac{q_{n2}}{k_{n2}}\,\beta_1(q_{n2}R)\,\frac{j_2(k_{n2}R)}{k_{n2}R}\right] \tag{32.b}$$

Numerical investigation of the behaviour of these coefficients shows that they decay asymptotically as n^{-2}:

$$a_{nl} \stackrel{n\to\infty}{\longrightarrow} \text{const} \times n^{-2} \tag{33}$$

Likewise, it is found that the frequencies ω_{n0} and ω_{n2} diverge like n for large n, so that $\mathbf{Z}^{(\alpha)}(\mathbf{x},\omega)$ drops as ω^{-3} for large ω. Figures 6 and 7 display a symbolic plot of $\omega^3\,\mathbf{Z}^{(00)}(\mathbf{x},\omega)$ and $\omega^3\,\mathbf{Z}^{(2m)}(\mathbf{x},\omega)$, respectively, which illustrates the situation: monopole modes soon reach the asymptotic regime, while there appear to be 3 sub-families of quadrupole modes regularly intertwined; the asymptotic regime for these sub-families is more irregularly reached. Note also the perfectly regular alternate changes of phase (by π radians) in both monopole and each quadrupole family.

The sharp fall in sensitivity of a sphere for higher frequency modes (n^{-3}) indicates that only the lowest ones stand a chance of being observable in an actual GW antenna. I report in Table I the numerical values of the relevant parameters for the first few monopole and quadrupole modes. The reason for the last (fourth) columns will become clear later.

4.2 The absorption cross section

Let us calculate now the energy of the oscillating sphere. We first define the *spectral energy density* at frequency ω, which is naturally given by[5]

[5] T is the integration time —assumed very large. The peaks in the δ-functions diverge like T/π.

Table 1: First few monopole (left) and quadrupole (right) sphere parameters, for a $\sigma = 0.33$ material. First and second columns on either side of the central line number the modes and give the corresponding eigenvalue; rows are intertwined in order of ascending frequency, which is proportional to kR —see (62) below. Third columns contain the a_{n0} and a_{n2} coefficients defined in equations (24); the fourth columns display the cross section *ratios* $(k_{10}a_{10}/k_{n0}a_{n0})^2$ and $(k_{12}a_{12}/k_{n2}a_{n2})^2$ for higher frequency modes, respectively, taking as reference the lowest in each family —cf. equations (47).

n	$k_{n0}R$	a_{n0}/R	σ_{10}/σ_{n0}	n	$k_{n2}R$	a_{n2}/R	σ_{12}/σ_{n2}
				1	2.650	0.328	1
				2	5.088	0.106	2.61
1	5.432	0.214	1				
				3	8.617	-1.907×10^{-2}	27.95
				4	10.917	-9.101×10^{-3}	76.42
2	12.138	-3.772×10^{-2}	6.46				
				5	12.280	1.387×10^{-2}	25.99
				6	15.347	6.879×10^{-3}	67.87
3	18.492	1.600×10^{-2}	15.49				

$$W(\omega) = \frac{1}{T}\int_{\text{Solid}} \frac{1}{2}\omega^2 \, |\mathbf{U}(\mathbf{x},\omega)|^2 \, \varrho \, d^3x \tag{34}$$

and can be easily evaluated:

$$W(\omega) = \frac{1}{2}\pi M \sum_{n=1}^{\infty} \sum_{l=0,2} \sum_{m=-l}^{l} a_{nl}^2 \left|G^{(lm)}(\omega)\right|^2 [\delta(\omega-\omega_{nl}) + \delta(\omega+\omega_{nl})] \tag{35}$$

The *energy* at any one spectral frequency ω_{nl} is obtained by *integration* of the spectral density in a narrow interval around $\omega = \pm\omega_{nl}$:

$$E(\omega_{nl}) = \int_{-\omega_{nl}-\varepsilon}^{-\omega_{nl}+\varepsilon} + \int_{\omega_{nl}-\varepsilon}^{\omega_{nl}+\varepsilon} W(\omega)\,\frac{d\omega}{2\pi} \tag{36}$$

In this case,

$$E(\omega_{nl}) = \frac{1}{2}\,M\,a_{nl}^2 \sum_{m=-l}^{l} \left|G^{(lm)}(\omega_{n2})\right|^2 \;, \qquad l = 0, 2 \tag{37}$$

The sensitivity parameter associated with the vibrational energy of the modes is the detector's *absorption cross section*, defined as the energy it absorbs per unit incident GW spectral flux density, or

$$\sigma_{\text{abs}}(\omega) = \frac{E(\omega)}{\Phi(\omega)} \tag{38}$$

where $\Phi(\omega)$ is the number of joules per square metre and Hz carried by the GW at frequency ω as it passes by the antenna. Thus, for the frequencies of interest,

$$\sigma_{\rm abs}(\omega_{n0}) \;=\; \frac{1}{2} M a_{n0}^2 \, \frac{\left| G^{(00)}(\omega_{n0}) \right|^2}{\Phi(\omega_{n0})} \tag{39.a}$$

$$\sigma_{\rm abs}(\omega_{n2}) \;=\; \frac{1}{2} M a_{n2}^2 \, \frac{\sum_{m=-2}^{2} \left| G^{(2m)}(\omega_{n2}) \right|^2}{\Phi(\omega_{n2})} \tag{39.b}$$

These quantities have very precise values, but such values can only be calculated on the basis of a *specific underlying theory of the GW physics*. In the absence of such theory, neither $\Phi(\omega)$ nor $G^{(lm)}(\omega)$ can possibly be calculated, since they are *not* theory independent quantities. To date, only GR calculations have been reported in the literature [13, 53, 61]. As I will now show, even though the fractions in the rhs of (39) are *not* theory independent, some very general results can still be obtained about the sphere's cross section within the context of metric theories of the gravitational interaction. To do so, it will be necessary to go into a short digression on the general nature of weak metric GWs.

No matter which is the (metric) theory which happens to be the "correct one" to describe gravitation, it is beyond reasonable doubt that any GWs reaching the Earth ought to be *very weak*. The linear approximation should therefore be an extremely good one to describe the propagating field variables in the neighbourhood of the detector. In such circumstances, the field equations can be derived from a Poincaré invariant variational principle based on an action integral of the type

$$\int \mathcal{L}(\psi_A, \psi_{A,\mu}) \, d^4x \tag{40}$$

where the Lagrangian density $\mathcal{L}$ is a *quadratic* functional of the field variables $\psi_A(x)$ and their space-time derivatives $\psi_{A,\mu}(x)$; these variables include the metric perturbations $h_{\mu\nu}$, plus any other fields required by the specific theory under consideration —e.g. a scalar field in the theory of Brans–Dicke, etc. The requirement that $\mathcal{L}$ be quadratic ensures that the Euler–Lagrange equations of motion are *linear*.

The energy and momentum transported by the waves can be calculated in this formalism in terms of the components $\tau^{\mu\nu}$ of the canonical energy-momentum tensor[6]

$$\tau^{\mu\nu}(\mathbf{x}, t) = \sum_A \frac{\partial \mathcal{L}}{\partial \psi_{A,\mu}} \, \psi_A^{,\nu} - \mathcal{L} \, \eta^{\mu\nu} \tag{41}$$

The flux energy density, or Poynting, vector is given by $S_i = c^2 \, \tau^{0i}$, i.e.,

$$\mathbf{S}(\mathbf{x}, t) = c^3 \sum_A \frac{\partial \mathcal{L}}{\partial \dot{\psi}_A} \, \nabla \psi_A \tag{42}$$

where $\dot{} \equiv \partial / \partial t$. Any GW hitting the antenna will be seen plane, due to the enormous distance to the source. If $\mathbf{k}$ is the incidence direction (normal to the wave front), then the fields will depend on the variable $ct - \mathbf{k}\cdot\mathbf{x}$, so that the GW energy reaching the detector per unit time and area is

$$\phi(t) \equiv \mathbf{k}\cdot\mathbf{S}(\mathbf{x}, t) = -c^2 \sum_A \frac{\partial \mathcal{L}}{\partial \dot{\psi}_A} \, \dot{\psi}_A \tag{43}$$

where $\mathbf{x}$ is the sphere's centre position relative to the source —which is *fixed*, and so its dependence can be safely dropped in the lhs of the above expression. The important thing to note in equation (43)

[6] This tensor is *not* symmetric in general, but can be symmetrized by a standard method due to Belinfante [7, 33]. For the considerations which follow in this paper it is unnecessary to go into those details, and the *canonical* form (41) will be sufficient.

is that it tells us that $\phi(t)$ *can be written as a quadratic form in the time derivatives of the fields* ψ_A. As a consequence, the spectral density $\Phi(\omega)$, defined by

$$\int_{-\infty}^{\infty} \phi(t)\, dt = \int_{0}^{\infty} \Phi(\omega)\, \frac{d\omega}{2\pi} \tag{44}$$

can be ascertained to factorise as

$$\Phi(\omega) = \omega^2\, \Phi_0(\omega) \tag{45}$$

where $\Phi_0(\omega)$ is again a *quadratic* function of the Fourier transforms $\Psi_A(\omega)$ of the fields ψ_A. On the other hand, the functions $G^{(lm)}(\omega)$ in (39) which, it is recalled, are the Fourier transforms of $g^{(lm)}(t)$ in (20), contain *second* order derivatives of the *metric* fields $h_{\mu\nu}$, and therefore of *all* the fields ψ_A as a result of the theory's field equations. Since we are considering *plane wave* solutions to those equations, all derivatives can be reduced to *time* derivatives —just like in (43) above. We can thus write

$$G^{(lm)}(\omega) = -\omega^2\, \Psi^{(lm)}(\omega) \tag{46}$$

with $\Psi^{(lm)}(\omega)$ suitable *linear* combinations of the $\Psi_A(\omega)$. Replacing the last two equations into (39) and manipulating dimensions expediently, we come to the remarkable result that

$$\sigma_{\rm abs}(\omega_{n0}) \;=\; K_S(\aleph)\, \frac{GMv_t^2}{c^3}\, (k_{n0}a_{n0})^2 \tag{47.a}$$

$$\sigma_{\rm abs}(\omega_{n2}) \;=\; K_Q(\aleph)\, \frac{GMv_t^2}{c^3}\, (k_{n2}a_{n2})^2 \tag{47.b}$$

where $v_t^2 \equiv (2{+}2\sigma)^{-1}\, v_{\rm s}^2$, $v_{\rm s}$ being the speed of sound in the detector's material, and σ its Poisson ratio; G is the Gravitational constant. The "remarkable" about the above is that the coefficients $K_S(\aleph)$ and $K_Q(\aleph)$ *are independent of frequency*: they *exclusively depend on the underlying gravitation theory*, which I symbolically denote by $\aleph$. To see that this is the case, it is enough to consider a monochromatic incident wave: since the coefficients $K_S(\aleph)$ and $K_Q(\aleph)$ happen to be *invariant* with respect to field amplitude *scalings*, this means they will *only* depend on the amplitudes' relative weights, i.e., on the field equations' *specific structure*.

By way of example, it is interesting to see what the results for General Relativity (GR) and Brans–Dicke (BD) theory are. After somehow lengthy algebra it is found that

$$\aleph = \text{GR} \Rightarrow \left\{ \begin{array}{l} K_S(\aleph) = 0 \\ \\ K_Q(\aleph) = \frac{16\,\pi^2}{15} \end{array} \right. \tag{48}$$

and

$$\aleph = \text{BD} \Rightarrow \left\{ \begin{array}{l} K_S(\aleph) = \frac{8\,\pi^2}{9}\, (3+2\Omega)^{-2}\, k\, \left[1 + \frac{k\Omega}{(3+2\Omega)^2}\right]^{-1} \\ \\ K_Q(\aleph) = \frac{16\,\pi^2}{15}\, \left[1 + \frac{1}{6}\, (3+2\Omega)^{-2}\, k\right] \left[1 + \frac{k\Omega}{(3+2\Omega)^2}\right]^{-1} \end{array} \right. \tag{49}$$

In the latter formulae, Ω is the usual Brans–Dicke parameter ω [11], renamed here to avoid confusion with *frequency*, and k is a dimensionless parameter, generally of order one, depending on the source's properties [36]. As is well known, GR is obtained in the limit $\Omega \to \infty$ of BD [62]; the quoted results are of course in agreement with that limit.

Incidentally, an interesting consequence of the above equations is that the presence of a scalar field in the theory of Brans and Dicke causes *not only the monopole* sphere's modes to be excited, *but also the* $m{=}0$ *quadrupole ones*; what we see in equations (49) is that *precisely* 5/6 of the total energy extracted

from the scalar wave goes into the antenna's monopole modes, whilst there is still a remaining 1/6 which is communicated to the quadrupoles, independently of the values of Ω and k[7].

This somehow non-intuitive result finds its explanation in the structure of the Riemann tensor in BD theory, in which the *excess* R_{0i0j} with respect to General Relativity happens *not* to be proportional to the scalar part $E_{ij}^{(00)}$, but to a combination of $E_{ij}^{(00)}$ and $E_{ij}^{(20)}$. More in-depth analysis of these facts has been investigated in reference [10].

Equations (47) show that, no matter which is the gravity theory assumed, the sphere's absorption cross sections for higher modes *scale* as the successive coefficients $(k_{n0}a_{n0})^2$ and $(k_{n2}a_{n2})^2$ for monopole and quadrupole modes, respectively. In particular, the result quoted in [13] that cross section for the second quadrupole mode is 2.61 times less than that for the first, assuming GR, is in fact valid, as we now see, *independently of which is the* (metric) *theory of gravity actually governing GW physics*. The fourth columns in Table 4.1 display these scaling properties. It is seen that the drop in cross section from the first to the second monopole mode is as high as 6.46. It should however be stressed that the frequency of such mode would be over 4 kHz for a (likely) sphere whose fundamental *quadrupole* frequency be 900 Hz [13]. Note finally the asymptotic cross section drop as n^{-2} for large n —cf. equation (33) and the ensuing paragraph.

5 Conclusion

The main purpose of this paper has been to set up a *sound* mathematical formalism to address with as much generality as possible any questions related to the interaction between a resonant antenna and a weak incoming GW, with much special emphasis on the homogeneous *sphere*. New results have been found along this line, such as the *scaling* properties of cross sections for higher frequency modes, or the sensitivity of the antenna to arbitrary metric GWs; also, new ideas have been put forward regarding the *direction deconvolution* problem within the context of an arbitrary metric theory of GW physics. Less spectacularly, the full machinery has also been applied to produce *independent* checks of previously published results.

The whole investigation reported herein has been developed with no *a priori* assumptions about any specific (metric) theory of the GWs, and is therefore *very* general. "Too general solutions" are often impractical in science; here, however, the "very general" appears to be rather "cheap", as seen in the results expressed by the equations of section 3 above. An immediate consequence is that solid elastic detectors of GWs (and, in particular, spheres) offer, as a matter of principle, the possibility of probing *any* given theory of GW physics with just as much effort as it would take, e.g., to probe General Relativity: the vector transfer function of section 4 supplies the requisite theoretical vehicle for the purpose.

An important question, however, has not been considered in this paper. This is the *transducer* problem: the sphere's oscillations can only be revealed to the observer by means of suitable (usually electromechanical) transducers. These devices, however, are not *neutral*, i.e., they *couple* to the antenna's motions, thereby exercising a back action on it which must be taken into consideration if one is to correctly interpret the system's readout. Preliminary studies and proposals have already been published [30], but further work is clearly needed for a more thorough understanding of the problems involved.

Progress in this direction is currently being made —which I expect to report on shortly. The formalism developed in this paper provides basic support to that further work[8].

[7] Note however that since monopole and quadrupole detector modes occur at different frequencies, this particular *distribution* of energy may not be seen if the sphere's vibrations are monitored at a single resonance.

[8] This *was* underway in 1995, and is now complete. The results are presented right below, from page 25 on.

Acknowledgments

It is a pleasure for me to thank Eugenio Coccia for his critical reading and comments on the manuscript. I also want to express gratitude to M Montero and JA Ortega for their assistance during the first stages of this work, and JMM Senovilla for some useful discussions. I have received support from the Spanish Ministry of Education through contract number PB93–1050.

Appendices

A.1 Algebra of the *E*-matrices

Let $\mathbf{e}_x, \mathbf{e}_y, \mathbf{e}_z$ be three orthonormal Cartesian vectors defining the sphere's laboratory reference frame. We define the equivalent triad

$$\mathbf{e}^{(0)} = \mathbf{e}_z \qquad , \qquad \mathbf{e}^{(\pm 1)} = \tfrac{1}{\sqrt{2}} \left(\mathbf{e}_x \pm i \mathbf{e}_y \right) \tag{50}$$

having the properties

$$\mathbf{e}^{*(m')} \cdot \mathbf{e}^{(m)} = \delta_{m'm} \qquad , \qquad m, m' = -1, 0, 1 \tag{51}$$

We say that the vectors (50) are the *natural basis* for the l=1 irreducible representation of the rotation group; they behave under arbitrary rotations precisely like the spherical harmonics $Y_{1m}(\mathbf{n})$. In particular, if a rotation of angle α around the z-axis is applied to the original frame then

$$\mathbf{e}^{(\pm 1)} \to \exp(\pm i\alpha)\, \mathbf{e}^{(\pm 1)} \qquad , \qquad \mathbf{e}^{(0)} \to \mathbf{e}^{(0)} \tag{52}$$

Higher rank tensors have specific multipole characteristics depending on the number of tensor indices, and the above basis lends itself to reveal those characteristics, too. For example, the five dimensional linear space of traceless symmetric tensors supports the l=2 irreducible representation of the rotation group, while a tensor's trace is an invariant. A general symmetric tensor can be expressed as an "orthogonal" sum of a traceless symmetric tensor and a multiple of the unit tensor. A convenient basis to expand any such tensor is the following:

$$\mathbf{e}^{(1)} \otimes \mathbf{e}^{(1)} \qquad , \qquad \mathbf{e}^{(-1)} \otimes \mathbf{e}^{(-1)} \tag{53.a}$$

$$\mathbf{e}^{(0)} \otimes \mathbf{e}^{(1)} + \mathbf{e}^{(1)} \otimes \mathbf{e}^{(0)} \quad , \quad \mathbf{e}^{(0)} \otimes \mathbf{e}^{(-1)} + \mathbf{e}^{(-1)} \otimes \mathbf{e}^{(0)} \tag{53.b}$$

$$\mathbf{e}^{(1)} \otimes \mathbf{e}^{(-1)} + \mathbf{e}^{(-1)} \otimes \mathbf{e}^{(1)} - 2\, \mathbf{e}^{(0)} \otimes \mathbf{e}^{(0)} \tag{53.c}$$

$$\mathbf{e}^{(1)} \otimes \mathbf{e}^{(-1)} + \mathbf{e}^{(-1)} \otimes \mathbf{e}^{(1)} + \mathbf{e}^{(0)} \otimes \mathbf{e}^{(0)} \tag{53.d}$$

The elements (53.a) get multiplied by $\mathrm{e}^{\pm 2i\alpha}$ in a rotation of angle α around the z-axis, respectively, the (53.b) by $\mathrm{e}^{\pm i\alpha}$, and (53.c) and (53.d) are invariant, as is readily seen. These properties define the "spin characteristics" of the corresponding tensors. Also, the five elements (53.a)–(53.c) are *traceless* tensors, while (53.d) is the *unit* tensor. Any symmetric tensor can be expressed as a linear combination of the six (53), and the respective coefficients carry the information about the weights of the different monopole and quadrupole components of the tensor.

Equations (16) in the text are the matrix representation of the above tensors in the Cartesian basis $\mathbf{e}_x, \mathbf{e}_y, \mathbf{e}_z$, except that they are multiplied by suitable coefficients to ensure that the conditions

$$E_{ij}^{(lm)}\, n_i n_j = Y_{lm}(\mathbf{n}) \;, \qquad l = 0, 2; \qquad m = -l, \ldots, l \tag{54}$$

where $\mathbf{n} \equiv \mathbf{x}/|\mathbf{x}|$ is the radial unit vector, hold. They are arbitrary, but expedient for the calculations in this paper. The following *orthogonality* relations can be easily established:

$$E^{*(2m')}_{ij}\,E^{(2m)}_{ij} = \tfrac{15}{8\pi}\,\delta_{m'm} \quad , \quad E^{*(00)}_{ij}\,E^{(2m)}_{ij} = 0 \quad , \quad E^{*(00)}_{ij}\,E^{(00)}_{ij} = \tfrac{3}{4\pi} \tag{55}$$

with the indices m,m' running from -2 to 2, and with an understood sum over the repeated i and j. It is also easy to prove the *closure* properties

$$E^{*(00)}_{ij}\,E^{(00)}_{kl} \;+\; \frac{2}{5}\sum_{m=-2}^{2} E^{*(2m)}_{ij}\,E^{(2m)}_{kl} = \tfrac{3}{8\pi}\,(\delta_{ik}\delta_{jl} + \delta_{il}\delta_{jk}) \tag{56}$$

Equations (55) and (56) constitute the *completeness* equations of the E-matrix basis of Euclidean symmetric tensors.

A.2 The sphere's spectrum and wave-functions

This Appendix is intended to give a rather complete summary of the frequency spectrum and eigenmodes of a uniform elastic sphere. Although this is a classical problem in Elasticity Theory [42], some of the results which follow have never been published so far. Also, its scope is to serve as reference for notation, etc., in future work —see ensuing article in page 25.

The uniform[9] elastic sphere's normal modes are obtained as the solutions to the eigenvalue equation

$$\mu\nabla^2\mathbf{u} + (\lambda+\mu)\,\nabla(\nabla\cdot\mathbf{u}) = -\omega^2\varrho\mathbf{u} \tag{57}$$

with the boundary conditions that its surface be free of any tensions and/or tractions; this is expressed by the equations [32]

$$\sigma_{ij}\,n_j = 0 \qquad \text{at} \quad r=R \tag{58}$$

where R is the sphere's radius, $\mathbf{n}$ the outward normal, and σ_{ij} the *stress* tensor

$$\sigma_{ij} = \lambda\,u_{kk}\delta_{ij} + 2\mu\,u_{ij} \tag{59}$$

with $u_{ij} \equiv \frac{1}{2}(u_{i,j} + u_{j,i})$, the *strain* tensor, and λ, μ the Lamé coefficients [32].

Like any differentiable vector field, $\mathbf{u}(\mathbf{x})$ can be expressed as a sum of an irrotational vector and a divergence-free vector,

$$\mathbf{u}(\mathbf{x}) = \mathbf{u}_{\text{irrot.}}(\mathbf{x}) + \mathbf{u}_{\text{div-free}}(\mathbf{x}) \;, \tag{60}$$

say; on substituting this into equation (57), and after a few easy manipulations, one can see that

$$(\nabla^2 + k^2)\,\mathbf{u}_{\text{div-free}}(\mathbf{x}) = 0 \;, \qquad (\nabla^2 + q^2)\,\mathbf{u}_{\text{irrot.}}(\mathbf{x}) = 0 \tag{61}$$

where

$$k^2 \equiv \frac{\varrho\omega^2}{\mu} \;, \qquad q^2 \equiv \frac{\varrho\omega^2}{\lambda+2\mu} \tag{62}$$

Now the irrotational component can generically be expressed as the *gradient* of a scalar function, i.e.,

$$\mathbf{u}_{\text{irrot.}}(\mathbf{x}) = \nabla\phi(\mathbf{x}) \tag{63}$$

while there are *two* linearly independent divergence-free components which, as can be readily verified, are

[9] By *uniform* I mean its density ϱ is constant throughout the solid in the unperturbed state.

$$\mathbf{u}^{(1)}_{\mathrm{div-free}}(\mathbf{x}) = \mathbf{L}\psi^{(1)}(\mathbf{x}) \ , \quad \text{and} \quad \mathbf{u}^{(2)}_{\mathrm{div-free}}(\mathbf{x}) = \nabla\times\mathbf{L}\psi^{(2)}(\mathbf{x}) \tag{64}$$

where $\mathbf{L} \equiv -i\mathbf{x}\times\nabla$ is the "angular momentum" operator, cf. [21], and $\psi^{(1)}$ and $\psi^{(2)}$ are also scalar functions. If (63) and (64) are now respectively substituted in (61), it is found that $\phi(\mathbf{x})$, $\psi^{(1)}(\mathbf{x})$, and $\psi^{(2)}(\mathbf{x})$ satisfy Helmholtz equations:

$$(\nabla^2 + k^2)\,\psi(\mathbf{x}) = 0 \ , \qquad (\nabla^2 + q^2)\,\phi(\mathbf{x}) = 0 \tag{65}$$

where $\psi(\mathbf{x})$ stands for either $\psi^{(1)}(\mathbf{x})$ or $\psi^{(2)}(\mathbf{x})$. Therefore

$$\phi(\mathbf{x}) = j_l(qr)\,Y_{lm}(\mathbf{n}) \qquad , \qquad \psi(\mathbf{x}) = j_l(kr)\,Y_{lm}(\mathbf{n}) \tag{66}$$

in order to ensure regularity at the centre of the sphere, r=0. Here, j_l is a *spherical* Bessel function —see [1] for general conventions on these functions—, and Y_{lm} a spherical harmonic [21]. Finally thus,

$$\mathbf{u}(\mathbf{x}) = \frac{C_0}{q^2}\,\nabla\phi(\mathbf{x}) + \frac{iC_1}{k}\,\mathbf{L}\psi(\mathbf{x}) + \frac{iC_2}{k^2}\,\nabla\times\mathbf{L}\psi(\mathbf{x}) \tag{67}$$

where C_0, C_1, C_2 are three constants which will be determined by the boundary conditions (58) (the denominators under them have been included for notational convenience). After lengthy algebra, those conditions can be expressed as the following system of linear equations:

$$\left[\beta_2(qR) - \tfrac{\lambda}{2\mu}\,q^2R^2\,\beta_0(qR)\right]\,C_0 - l(l+1)\,\beta_1(kR)\,C_2 \;=\; 0 \tag{68.a}$$

$$\beta_1(kR)\,C_1 \;=\; 0 \tag{68.b}$$

$$\beta_1(qR)\,C_0 - \left[\tfrac{1}{2}\,\beta_2(kR) + \left\{\tfrac{l(l+1)}{2} - 1\right\}\,\beta_0(kR)\right]\,C_2 \;=\; 0 \tag{68.c}$$

where

$$\beta_0(z) \equiv \frac{j_l(z)}{z^2} \ , \quad \beta_1(z) \equiv \frac{d}{dz}\left[\frac{j_l(z)}{z}\right] \ , \quad \beta_2(z) \equiv \frac{d^2}{dz^2}\left[j_l(z)\right] \tag{69}$$

There are clearly *two* families of solutions to (68):

i) *Toroidal* modes. These are characterised by

$$\beta_1(kR) = 0 \ , \qquad C_0 = C_2 = 0 \tag{70}$$

The frequencies of these modes are *independent* of λ, and thence independent of the material's Poisson ratio. Their amplitudes are

$$\mathbf{u}^T_{nlm}(\mathbf{x}) = T_{nl}(r)\,i\mathbf{L}Y_{lm}(\mathbf{n}) \tag{71}$$

with

$$T_{nl}(r) = C_1(n,l)\,j_l(k_{nl}r) \tag{72}$$

and $C_1(n,l)$ a dimensionless normalisation constant determined by the general formula (8); $k_{nl}R$ is the n-th root of the first equation (70) for a given l.

ii) *Spheroidal* modes. These correspond to

$$\det\left(\begin{array}{cc} \beta_2(qR)-\frac{\lambda}{2\mu}\,q^2R^2\,\beta_0(qR) & l(l+1)\,\beta_1(kR) \\ \beta_1(qR) & \frac{1}{2}\,\beta_2(kR)+\left\{\frac{l(l+1)}{2}-1\right\}\,\beta_0(kR) \end{array}\right)=0 \tag{73}$$

and $C_1=0$. The frequencies of these modes *do* depend on the Poisson ratio, and their amplitudes are

$$\mathbf{u}^P_{nlm}(\mathbf{x}) = A_{nl}(r)\,Y_{lm}(\mathbf{n})\,\mathbf{n} - B_{nl}(r)\,i\mathbf{n}\times\mathbf{L}Y_{lm}(\mathbf{n}) \tag{74}$$

where $A_{nl}(r)$ and $B_{nl}(r)$ have the somewhat complicated form

$$A_{nl}(r) \;=\; C(n,l)\left[\beta_3(k_{nl}R)\,j_l'(q_{nl}r) - l(l+1)\,\frac{q_{nl}}{k_{nl}}\,\beta_1(q_{nl}R)\,\frac{j_l(k_{nl}r)}{k_{nl}r}\right] \tag{75.a}$$

$$B_{nl}(r) \;=\; C(n,l)\left[\beta_3(k_{nl}R)\,\frac{j_l(q_{nl}r)}{q_{nl}r} - \frac{q_{nl}}{k_{nl}}\,\beta_1(q_{nl}R)\,\frac{\{k_{nl}r\,j_l(k_{nl}r)\}'}{k_{nl}r}\right] \tag{75.b}$$

with accents denoting derivatives with respect to implied (dimensionless) arguments,

$$\beta_3(z)\equiv\tfrac{1}{2}\,\beta_2(z)+\left\{\tfrac{l(l+1)}{2}-1\right\}\,\beta_0(z) \tag{76}$$

and $C(n,l)$ a new normalisation constant. It is understood that q_{nl} and k_{nl} are obtained after the (transcendental) equation (73) has been solved for ω —cf. equation (62).

In actual practice equations (70) and (73) are solved for the *dimensionless* quantity kR, which will hereafter be called the *eigenvalue*. In view of (62), the relationship between the latter and the measurable frequencies (in Hz) is given by

$$\nu\equiv\frac{\omega}{2\pi}=\left(\frac{\mu}{\varrho\,R^2}\right)^{1/2}\,\frac{kR}{2\pi} \tag{77}$$

It is more useful to express the frequencies in terms of the Poisson ratio, σ, and of the speed of sound $v_{\rm s}$ in the selected material. For this the following formulas are required —see e.g. [32]:

$$v_{\rm s}=\sqrt{\frac{\mathsf{Y}}{\varrho}} \tag{78}$$

where Y is the *Young modulus*, related to the Lamé coefficients and the Poisson ratio by

$$\mathsf{Y}=\frac{(3\lambda+2\mu)\,\mu}{\lambda+\mu}=2\,(1+\sigma)\,\mu\;,\qquad \sigma\equiv\frac{\lambda}{2(\lambda+\mu)} \tag{79}$$

Hence,

$$\nu=\frac{(kR)}{2\pi\,\sqrt{1+\sigma}}\,\frac{v_{\rm s}}{R} \tag{80}$$

Equation (80) provides a suitable transformation formula from abstract number eigenvalues (kR) into physical frequencies ν, for given material's properties and sizes.

Tables 3 and 2 respectively display a set of values of (kR) for *toroidal* and *spheroidal* modes. While GWs can only couple to quadrupole and monopole modes, it is important to have some detailed knowledge of analytical results, as the sphere's frequency spectrum is rather involved. It often happens, both

Table 2: List of a few *spheroidal eigenvalues*, ordered in columns of ascending harmonics for each multipole value. Spheroidal eigenvalues depend on the sphere's material Poisson ratio —although this dependence is weak. In this table, values are given for $\sigma = 0.33$. Note that the table contains *all* eigenvalues less than or equal to 11.024 yet is not exhaustive for values larger than that one; this would require to stretch the table horizontally beyond $l = 10$ —see Figure I for a qualitative inspection of trends in eigenvalue progressions.

n	$l=0$	$l=1$	$l=2$	$l=3$	$l=4$	$l=5$	$l=6$	$l=7$	$l=8$	$l=9$	$l=10$
1	5.4322	3.5895	2.6497	3.9489	5.0662	6.1118	7.1223	8.1129	9.0909	10.061	11.024
2	12.138	7.2306	5.0878	6.6959	8.2994	9.8529	11.340	12.757	14.111	15.410	16.665
3	18.492	8.4906	8.6168	9.9720	11.324	12.686	14.066	15.462	16.867	18.272	19.664
4	24.785	10.728	10.917	12.900	14.467	15.879	17.243	18.589	19.930	21.272	22.619
5	31.055	13.882	12.280	14.073	16.125	18.159	19.997	21.594	23.043	24.426	25.778

in numerical simulations and in experimental determinations, that it is very difficult to disentangle the wealth of observed frequency lines, and to correctly associate them with the corresponding eigenmode. Complications are further enhanced by partial degeneracy lifting found in practice (due to broken symmetries), which result in even more frequency lines in the spectrum. Accurate analytic results should therefore be very helpful to assist in frequency identification tasks.

Table 3: List of a few *toroidal eigenvalues*, ordered in columns of ascending harmonics for each multipole value. Unlike spheroidal eigenvalues, toroidal eigenvalues are independent of the sphere's material Poisson ratio. Note that the table contains *all* eigenvalues less than or equal to 12.866 yet is not exhaustive for values larger than that one; this would require to stretch the table horizontally beyond $l = 11$ —see Figure II for a qualitative inspection of trends in eigenvalue progressions.

n	$l=1$	$l=2$	$l=3$	$l=4$	$l=5$	$l=6$	$l=7$	$l=8$	$l=9$	$l=10$	$l=11$
1	5.7635	2.5011	3.8647	5.0946	6.2658	7.4026	8.599	9.6210	10.711	11.792	12.866
2	9.0950	7.1360	8.4449	9.7125	10.951	12.166	13.365	14.548	15.720	16.882	18.035
3	12.323	10.515	11.882	13.211	14.511	15.788	17.045	18.287	19.515	20.731	21.937
4	15.515	13.772	15.175	16.544	17.886	19.204	20.503	21.786	23.055	24.310	25.555
5	18.689	16.983	18.412	19.809	21.181	22.530	23.860	25.174	26.473	27.760	29.035

In Figures 1 and 2 a symbolic line diagramme of the two families of frequencies of the sphere's spectrum is presented. Spheroidal eigenvalues have been plotted for the Poisson ratio σ=0.33. Although only the l=0 and l=2 *spheroidal* series couple to GW tidal forces, the plots include other eigenvalues, as they can be useful both in bench experiments —cf. equation (12) above— and for vetoing purposes in a spherical antenna.

Figures 3, 4 and 5 contain plots of the first three monopole and quadrupole functions $T_{nl}(r)$, $A_{nl}(r)$ and $B_{nl}(r)$, always for σ=0.33. $T_{n0}(r)$ and $B_{n0}(r)$ have however been omitted; this is because they are multiplied by an identically zero angular coefficient in the amplitude formulae (71) and (74). Indeed, monopole vibrations are spherically symmetric, i.e., purely radial.

List of Figures

Figure I The homogeneous sphere *spheroidal* eigenvalues for a few *multipole* families. Only the l=0 and l=2 families couple to metric GWs, so the rest are given for completeness and non-directly-GW uses. Note that there are *fewer* monopole than any other l-pole modes. The lowest frequency is the first *quadrupole*. The diagram corresponds to a sphere with Poisson ratio σ=0.33. Frequencies can be obtained from the plotted values through equation (80) for any specific case.

Figure II The homogeneous sphere *toroidal* eigenvalues. None of these couple to GWs, but knowledge of them can be useful for *vetoing* purposes. These eigenvalues are *independent* of the material's Poisson ratio. To obtain actual frequencies from plotted values, use (80). The lowest *toroidal* eigenvalue is $kR = 2.5011$, with l=2, and happens to be the *absolute minimum* sphere's eigenvalue. Compared to the *spheroidal* $kR = 2.6497$, also with l=2, its frequency is 5.61% smaller. Note also that there are no monopole toroidal modes.

Figure III First three *spheroidal monopole* radial functions $A_{n0}(r)$ $(n = 1, 2, 3)$, equation (75.a).

Figure IV First three *spheroidal quadrupole* radial functions $A_{n2}(r)$ (continuous line) and $B_{n2}(r)$ (broken line) $(n = 1, 2, 3)$, equations (75).

Figure V First three *toroidal quadrupole* radial functions $T_{n2}(r)$ $(n = 1, 2, 3)$, equation (72). A common feature to these radial functions (also in the two previous Figures) is that they present a *nodal* point at the origin $(r = 0)$, while the sphere's surface $(r/R = 1)$ has a non-zero amplitude value, which is largest (in absolute value) for the lowest n in each group.

Figure VI The *scalar* component $\mathbf{Z}^{(00)}(\mathbf{x}, \omega)$ of the *multimode* transfer function, (31.a). The diagram actually displays $\omega^3\, \mathbf{Z}^{(00)}(\mathbf{x}, \omega)$, so asymptotic behaviours are better appreciated. It is given in units of $\mu/\varrho R$, and a factor $(\pi/i)\, \mathbf{u}_{n00}(\mathbf{x})$, the eigenmode amplitude, has been omitted, too. δ-function amplitudes are symbolically taken as 1. Note that the asymptotic regime, given by equation (33), is quickly reached.

Figure VII The *quadrupole* component $\mathbf{Z}^{(2m)}(\mathbf{x}, \omega)$ of the *multimode* transfer function, (31.b). The same prescriptions of Figure 6 apply here; the plot is therefore *independent* of the value of m. Note the presence of *three* sub-families of peaks; asymptotic regimes are reached with variable speed for these sub-families, and less rapidly than for monopole modes, anyway.

Spheroidal spectrum

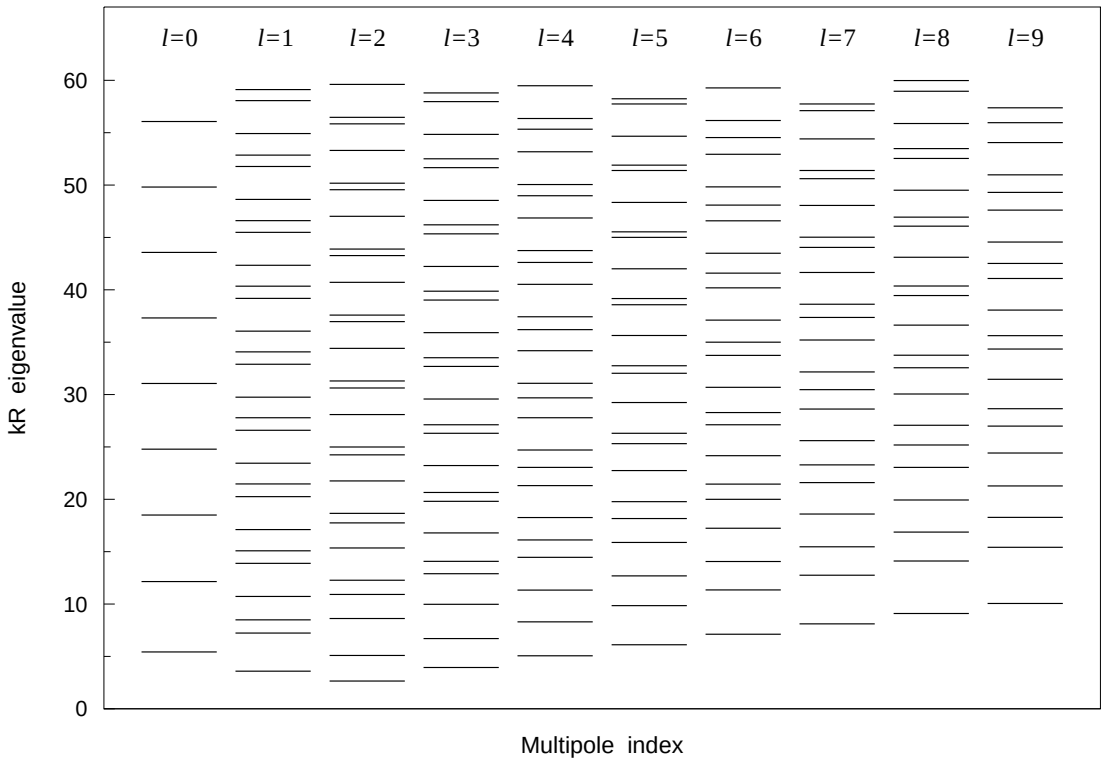

FIG. I

Toroidal spectrum

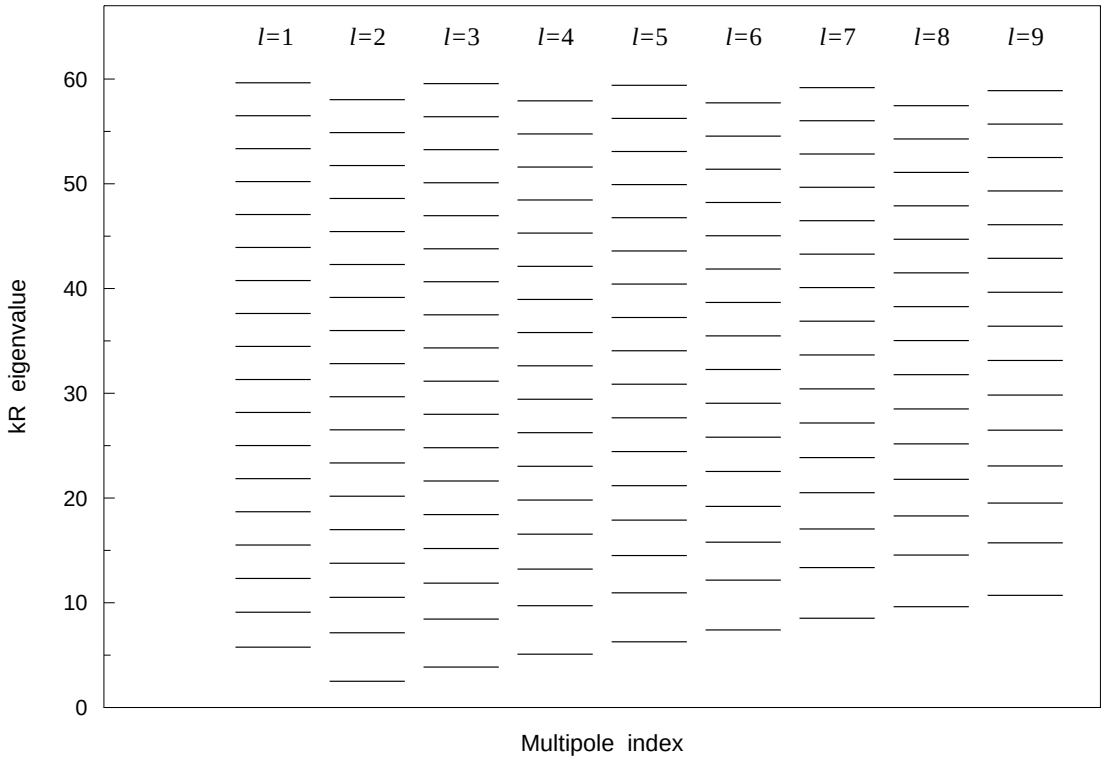

FIG. II

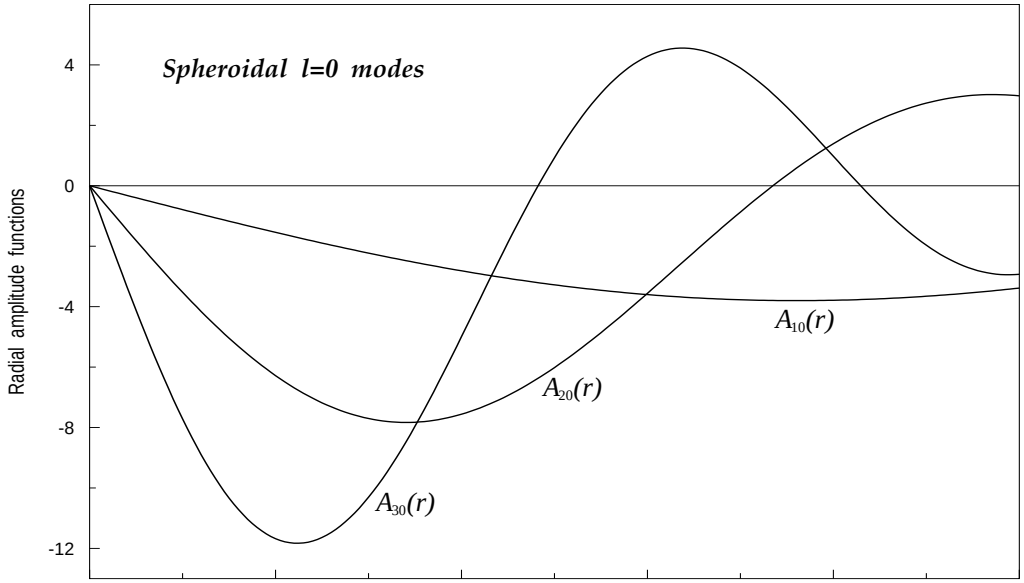

FIG. III

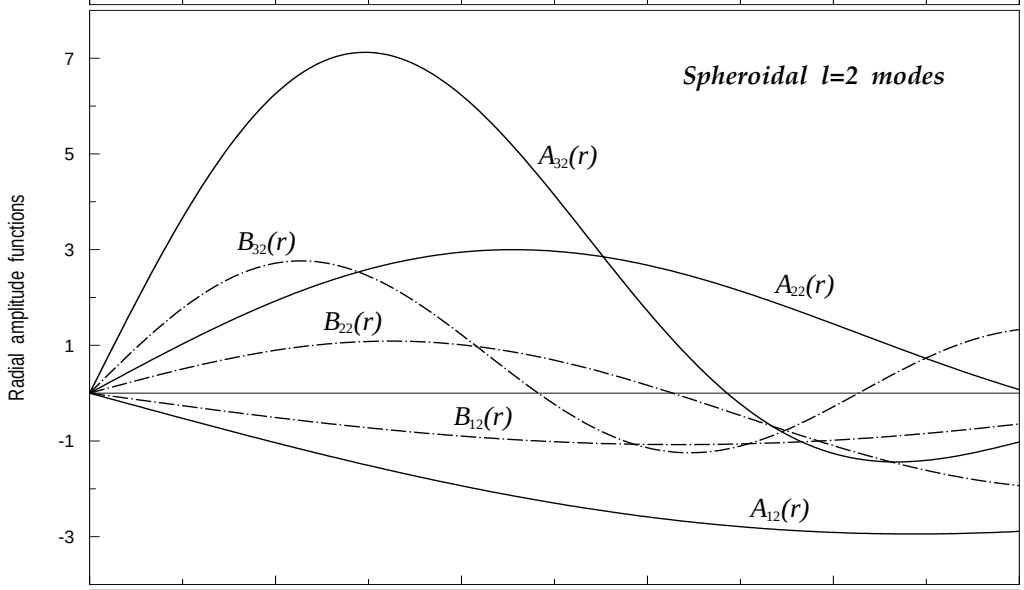

FIG. IV

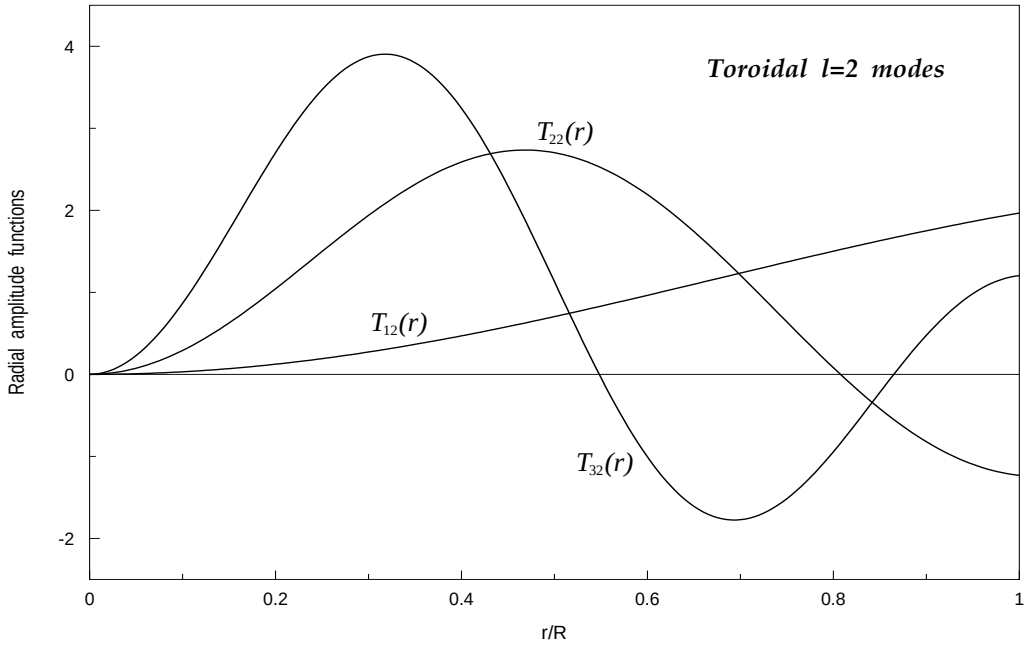

FIG. V

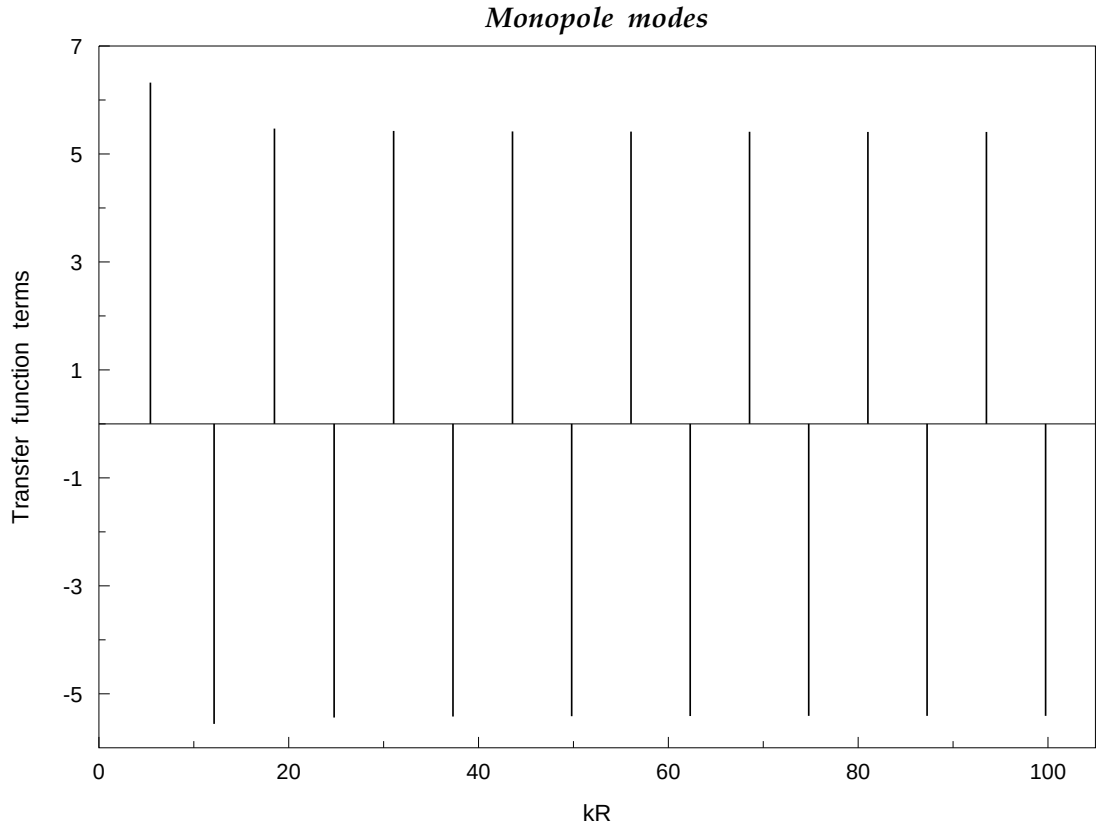

FIG. VI

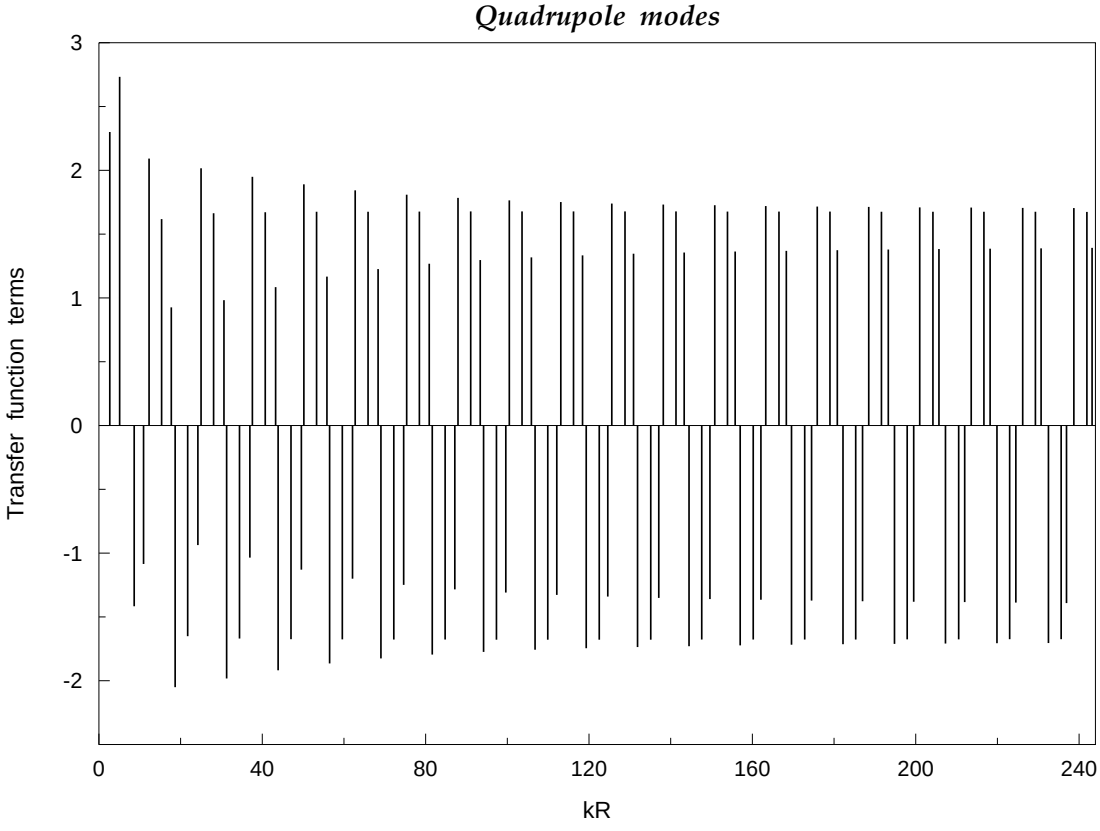

FIG. VII

Multiple mode gravitational wave detection with a spherical antenna

MNRAS **316**, 173-194 (2000)

José Alberto Lobo

Departament de Física Fonamental
Universitat de Barcelona, Spain
e-mail: lobo@hermes.ffn.ub.es

Abstract

Apart from omnidirectional, a solid elastic sphere is a natural multi-mode and multi-frequency device for the detection of Gravitational Waves (GW). Motion sensing in a spherical GW detector thus requires a *multiple* set of transducers attached to it at suitable locations. If these are *resonant* then they exert a significant back action on the larger sphere and, as a consequence, the *joint dynamics* of the entire system must be properly understood before reliable conclusions can be drawn from its readout. In this paper, I present and develop an analytic approach to study such dynamics which generalises currently existing ones and clarifies their actual range of validity. In addition, the new formalism shows that there actually exist resonator layouts alternative to the highly symmetric *TIGA*, potentially having interesting properties. One of these (I will call it *PHC*), which only requires five resonators per quadrupole mode sensed, and has *mode channels*, will be described in detail. Also, the *perturbative* nature of the proposed approach makes it very well adapted to systematically assess the consequences of realistic mistunings in the device parameters by robust analytic methods. In order to check the real value of the mathematical model, its predictions have been confronted with experimental data from the *LSU* prototype detector *TIGA*, and agreement between both is found to consistently reach a satisfactory precision of *four* decimal places.

1 Introduction

The idea of using a solid elastic sphere as a gravitational wave (GW) antenna is almost as old as that of using cylindrical bars: as far back as 1971 Forward published a paper [22] in which he assessed some of the potentialities offered by a spherical solid for that purpose. It was however Weber's ongoing philosophy and practice of using bars which eventually prevailed and developed up to the present date, with the highly sophisticated and sensitive ultra-cryogenic systems currently in operation —see [14] and [16] for reviews and bibliography. With few exceptions [2, 61], spherical detectors fell into oblivion for years, but interest in them strongly re-emerged in the early 1990's, and an important number of research articles have been published since which address a wide variety of problems in GW spherical detector science. At the same time, international collaboration has intensified, and prospects for the actual construction of large spherical GW observatories (in the range of $\sim$100 tons) are being currently considered in several countries [10], even in a variant *hollow* shape [17].

A spherical antenna is obviously omnidirectional but, most important, it is also a natural *multi-mode* device, i.e., when suitably monitored, it can generate information on all the GW amplitudes and incidence direction [43], a capability which possesses no other *individual* GW detector, whether resonant or interferometric [19]. Furthermore, a spherical antenna could also reveal the eventual existence of *monopole* gravitational radiation, or set thresholds on it [10].

The theoretical explanation of these facts is to be found in the unique matching between the GW amplitude structure and that of the sphere oscillation eigenmodes [39, 41]: a general *metric* GW generates a *tidal* field of forces in an elastic body which is given in terms of the "electric" components $R_{0i0j}(t)$ of the Riemann tensor at its centre of mass by the following formula, see equation (19) above [37]:

[10] There are collaborations in Brazil, Holland, Italy and Spain.

$$\mathbf{f}_{\rm GW}(\mathbf{x},t) \quad = \sum_{\substack{l=0 \text{ and } 2 \\ m=-l,\ldots,l}} \mathbf{f}^{(lm)}(\mathbf{x})\, g^{(lm)}(t) \tag{81}$$

where $\mathbf{f}^{(lm)}(\mathbf{x})$ are "tidal form factors", while $g^{(lm)}(t)$ are specific linear combinations of the Riemann tensor components $R_{0i0j}(t)$ which carry all the *dynamical* information on the GW's monopole ($l=0$) and quadrupole ($l=2$) amplitudes. It is precisely these amplitudes, $g^{(lm)}(t)$, which a GW detector aims to measure.

On the other hand, a free elastic sphere has two families of oscillation eigenmodes, so called *toroidal* and *spheroidal* modes, and modes within either family group into ascending series of l-pole harmonics, each of whose frequencies is $(2l+1)$-fold degenerate —see [37] for full details. It so happens that *only* monopole and/or quadrupole spheroidal modes can possibly be excited by an incoming *metric* GW [9], and their GW driven amplitudes are directly proportional to the wave amplitudes $g^{(lm)}(t)$ of equation (81). It is this very fact which makes of the spherical detector such a natural one for GW observations [37]. In addition, a spherical antenna has a significantly higher absorption *cross section* than a cylinder of like fundamental frequency, and also presents good sensitivity at the *second* quadrupole harmonic [13].

In order to monitor the GW induced deformations of the sphere *motion sensors* are required. In cylindrical bars, current state of the art technology is based upon *resonant transducers* [4, 24]. A resonant transducer consists in a small (compared to the bar) mechanical device possessing a resonance frequency accurately tuned to that of the cylinder. This *frequency matching* causes back-and-forth *resonant energy transfer* between the two bodies (bar and resonator), which results in turn in *mechanically amplified* oscillations of the smaller resonator. The philosophy of using resonators for motion sensing is directly transplantable to a spherical detector —only a *multiple* set rather than a single resonator is required if its potential capabilities as a multi-mode system are to be exploited to satisfaction.

A most immediate question in a multiple motion sensor system is: *where* should the sensors be? The answer to this basic question naturally depends on design and purpose criteria. Merkowitz and Johnson (M&J) made a very appealing proposal consisting in a set of 6 identical resonators coupling to the *radial* motions of the sphere's surface, and occupying the positions of the centres of the 6 non-parallel pentagonal faces of a truncated icosahedron [30, 46]. One of the most remarkable properties of such layout is that there exist 5 linear combinations of the resonators' readouts which are directly proportional to the 5 quadrupole GW amplitudes $g^{(2m)}(t)$ of equation (81). M&J call these combinations *mode channels*, and they therefore play a fundamental role in GW signal deconvolution in a real, *noisy* system [49, 51]. In addition, a reduced scale prototype antenna —called *TIGA*, for *T*runcated *I*cosahedron *G*ravitational *A*ntenna— was constructed at Louisiana State University, and its working experimentally put to test [45]. The remarkable success of this experiment in almost every detail [47, 48, 50] stands as a vivid proof of the practical feasibility of a spherical GW detector [6, 52].

Despite its success, the theoretical model proposed by M&J to describe the system dynamics is based upon a simplifying assumption that the resonators *only* couple to to the quadrupole vibration modes of the sphere [30, 46]. While this is seen *a posteriori* of experimental measurements to be a very good approximation [45, 48], a deeper *physical* reason which explains *why* this happens is missing so far. The original motivation for the research I present in this article was to develop a more general approach, based on first principles, for the analysis of the resonator problem, very much in the spirit of the methodology and results of reference [37]; this, I thought, would not only provide the necessary tools for a rigorous analysis of the system dynamics, but also contribute to improve our understanding of the physics of the spherical GW detector.

Pursuing this programme, I succeeded in setting up and solving the equations of motion for the coupled system of sphere plus resonators. The most important characteristic of the solution is that it is expressible as a *perturbative series expansion in ascending powers of the small parameter* $\eta^{1/2}$, where η is the ratio between the average resonator's mass and the sphere's mass. The dominant (lowest)

order terms in this expansion appear to exactly reproduce Merkowitz and Johnson's equations [46], whence a quantitative assessment of their degree of accuracy, as well as of the range of validity of their underlying hypotheses obtains; if further precision is required then a well defined procedure for going to next (higher) order terms is unambiguously prescribed by the system equations.

Beyond this, though, the simple and elegant algebra which emerges out of the general scheme has enabled the exploration of different resonator layouts, alternative to the unique *TIGA* of M&J. In particular, I found one [38, 40] requiring 5 rather than 6 resonators per quadrupole mode sensed and possessing the remarkable property that *mode channels* can be constructed from the system readouts, i.e., five linear combinations of the latter which are directly proportional to the five quadrupole GW amplitudes. I called this distribution *PHC* —see below for full details.

The intrinsically perturbative nature of the proposed approach makes it also particularly well adapted to assess the consequences of small defects in the system structure, such as for example symmetry breaking due to suspension attachments, small resonator mistunings and mislocations, etc. This has been successfully applied to account for the reported frequency measurements of the *LSU TIGA* prototype [45], which was diametrically drilled for suspension purposes; in particular, discrepancies between measured and calculated values (generally affecting only the *fourth* decimal place) are precisely of the theoretically predicted order of magnitude.

The method has also been applied to analyse the stability of the spherical detector to several mistuned parameters, with the result that it is not very sensitive to small construction errors. This conforms again to experimental reports [50], but has the advantage that the argument depends on *analytic* mathematical work rather than on computer simulated procedures —see e.g. [50] or [58].

The paper is structured as follows: in section 2, I present the main physical hypotheses of the model, and the general equations of motion. In section 3 a Green function approach to solve those equations is set up, and in section 4 it is used to assess the system response to both monopole and quadrupole GW signals. In section 5 I describe in detail the *PHC* layout, including its frequency spectrum and *mode channels*. Section 6 contains a few brief considerations on the system response to a hammer stroke calibration signal, and finally in section 7 I assess how the different parameter mistunings affect the detector's behaviour. The paper closes with a summary of conclusions, and three appendices where the heavier mathematical details are made precise for the interested reader.

2 General equations

With minor improvements, I shall use the notation of references [37] and [38], some of which is now briefly recalled. Consider a solid sphere of mass $\mathcal{M}$, radius R, (uniform) density ϱ, and elastic Lamé coefficients λ and μ, endowed with a set of J resonators of masses M_a and resonance frequencies Ω_a ($a=1,\ldots,J$), respectively. I shall model the latter as *point masses* attached to one end of a linear spring, whose other end is rigidly linked to the sphere at locations $\mathbf{x}_a$ —see Figure 2. The system degrees of freedom are given by the *field* of elastic displacements $\mathbf{u}(\mathbf{x},t)$ of the sphere plus the *discrete* set of resonator spring deformations $z_a(t)$; equations of motion need to be written down for them, of course, and this is my next concern in this section.

I shall assume that the resonators only move radially, and also that Classical Elasticity theory [32] is sufficiently accurate for the present purposes[11]. In these circumstances we thus have

$$\varrho\,\frac{\partial^2\mathbf{u}}{\partial t^2} \;=\; \mu\nabla^2\mathbf{u} + (\lambda+\mu)\,\nabla(\nabla\cdot\mathbf{u}) + \mathbf{f}(\mathbf{x},t) \tag{82.a}$$

$$\ddot{z}_a(t) \;=\; -\Omega_a^2\,[z_a(t)-u_a(t)] + \xi_a^{\text{external}}(t)\;, \qquad a=1,\ldots,J \tag{82.b}$$

[11] We clearly do not expect relativistic motions in extremely small displacements at typical frequencies in the range of 1 kHz.

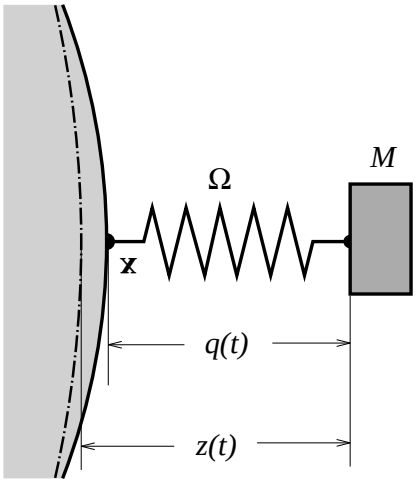

Figure 1: Schematic diagram of the coupling model between a solid sphere and a resonator. The notation is that in the text, but sub-indices have been dropped for clarity. The dashed-dotted arc line on the left indicates the position of the *undeformed* sphere's surface, and the solid arc its *actual* position.

where $\mathbf{n}_a \equiv \mathbf{x}_a/R$ is the outward pointing normal at the the a-th resonator's attachment point, and

$$u_a(t) \equiv \mathbf{n}_a \cdot \mathbf{u}(\mathbf{x}_a, t) \ , \qquad a = 1, \ldots, J \tag{83}$$

is the *radial* deformation of the sphere's surface at $\mathbf{x}_a$. A dot ($\dot{}$) is an abbreviation for time derivative. The term in square brackets in (82.b) is thus the spring deformation —$q(t)$ in Figure 2.

$\mathbf{f}(\mathbf{x}, t)$ in the rhs of (82.a) contains the *density* of all *non-internal* forces acting on the sphere, which is expediently split into a component due the resonators' *back action* and an external action *proper*, which can be a GW signal, a calibration signal, etc. Then

$$\mathbf{f}(\mathbf{x}, t) = \mathbf{f}_{\text{resonators}}(\mathbf{x}, t) + \mathbf{f}_{\text{external}}(\mathbf{x}, t) \tag{84}$$

Finally, $\xi_a^{\text{external}}(t)$ in the rhs of (82.b) is the force per unit mass (acceleration) acting on the a-th resonator due to *external* agents.

Given the hypothesis that the resonators are *point masses*, the following holds:

$$\mathbf{f}_{\text{resonators}}(\mathbf{x}, t) = \sum_{a=1}^{J} M_a \Omega_a^2 \ [\, z_a(t) - u_a(t)] \ \delta^{(3)}(\mathbf{x} - \mathbf{x}_a)\, \mathbf{n}_a \tag{85}$$

where $\delta^{(3)}$ is the three dimensional Dirac density function.

The *external* forces I shall be considering in this paper will be *gravitational wave* signals, and also a simple calibration signal, a perpendicular *hammer stroke*. GW driving terms, c.f. equation (81), can be written

$$\mathbf{f}_{\text{GW}}(\mathbf{x}, t) = \mathbf{f}^{(00)}(\mathbf{x})\, g^{(00)}(t) \ + \ \sum_{m=-2}^{2} \mathbf{f}^{(2m)}(\mathbf{x})\, g^{(2m)}(t) \tag{86}$$

for a general *metric* wave —see [37] for explicit formulas and technical details. While the spatial coefficients $\mathbf{f}^{(lm)}(\mathbf{x})$ are pure *form factors* associated to the *tidal* character of a GW excitation, it is the time dependent factors $g^{(lm)}(t)$ which carry the specific information on the incoming GW. The purpose of a GW detector is to determine the latter coefficients on the basis of suitable measurements.

If a GW sweeps the observatory then the resonators themselves will also be affected, of course. They will be driven, relative to the sphere's centre, by a tidal acceleration which, since they only move radially, is given by

$$\xi_a^{\rm GW}(t) = c^2\, R_{0i0j}(t)\, x_{a,i} n_{a,j} \ , \qquad a = 1, \ldots, J \tag{87}$$

where $R_{0i0j}(t)$ are the "electric" components of the GW Riemann tensor at the centre of the sphere. These can be easily manipulated to give[12]

$$\xi_a^{\rm GW}(t) = R \sum_{\substack{l=0 \text{ and } 2 \\ m=-l,\ldots,l}} Y_{lm}(\mathbf{n}_a)\, g^{(lm)}(t) \ , \qquad a = 1, \ldots, J \tag{88}$$

where R is the sphere's radius.

I shall also be later considering the response of the system to a particular *calibration* signal, consisting in a hammer stroke with intensity $\mathbf{f}_0$, delivered perpendicularly to the sphere's surface at point $\mathbf{x}_0$:

$$\mathbf{f}_{\rm stroke}(\mathbf{x}, t) = \mathbf{f}_0\, \delta^{(3)}(\mathbf{x} - \mathbf{x}_0)\, \delta(t) \tag{89}$$

which is modeled as an impulsive force in both space and time variables. Unlike GW tides, a hammer stroke will be applied on the sphere's surface, so it has no *direct* effect on the resonators. In other words,

$$\xi_a^{\rm stroke}(t) = 0 \ , \qquad a = 1, \ldots, J \tag{90}$$

The fundamental equations thus finally read:

$$\begin{aligned} \varrho \frac{\partial^2 \mathbf{u}}{\partial t^2} &= \mu \nabla^2 \mathbf{u} + (\lambda + \mu)\, \nabla(\nabla \cdot \mathbf{u}) + \\ &\quad \sum_{b=1}^{J} M_b \Omega_b^2\, [z_b(t) - u_b(t)]\, \delta^{(3)}(\mathbf{x} - \mathbf{x}_b)\, \mathbf{n}_b + \mathbf{f}_{\rm external}(\mathbf{x}, t) \end{aligned} \tag{91.a}$$

$$\ddot{z}_a(t) = -\Omega_a^2\, [z_a(t) - u_a(t)] + \xi_a^{\rm external}(t) \ , \qquad a = 1, \ldots, J \tag{91.b}$$

where $\mathbf{f}_{\rm external}(\mathbf{x}, t)$ will be given by either (86) or (89), as the case may be. Likewise, $\xi_a^{\rm external}(t)$ will be given by (88) or (90), respectively. The remainder of this paper will be concerned with finding solutions to the system of coupled differential equations (91), and with their meaning and consequences.

3 Green function formalism

In order to solve equations (91) I shall resort to Green function formalism. The essentials of this procedure in the context of the present problem can be found in detail in reference [37]; more specific technicalities are given in appendix A.1.

By means of such formalism equations (91) become the following integro-differential system:

$$u_a(t) = u_a^{\rm external}(t) + \sum_{b=1}^{J} \eta_b \int_0^t K_{ab}(t - t')\, \left[\, z_b(t') - u_b(t') \right]\, dt' \tag{92.a}$$

$$\ddot{z}_a(t) = \xi_a^{\rm external}(t) - \Omega_a^2\, \left[\, z_a(t) - u_a(t) \right] \ , \qquad a = 1, \ldots, J \tag{92.b}$$

[12] $Y_{lm}(\mathbf{n})$ are spherical harmonics [21] —see also the multipole expansion of $R_{0i0j}(t)$ in reference [37].

where $u_a^{\text{external}}(t) \equiv \mathbf{n}_a \cdot \mathbf{u}^{\text{external}}(\mathbf{x}_a, t)$, and $\mathbf{u}^{\text{external}}(\mathbf{x}, t)$ is the *bare* (i.e., without attached resonators) sphere's response to the external forces $\mathbf{f}_{\text{external}}(\mathbf{x}, t)$ in the rhs of (91.a). $K_{ab}(t)$ is a *kernel matrix* defined by the following weighted sum of diadic products of wavefunctions[13]:

$$K_{ab}(t) = \Omega_b^2 \sum_N \omega_N^{-1} \, [\mathbf{n}_b \cdot \mathbf{u}_N^*(\mathbf{x}_b)] \, [\mathbf{n}_a \cdot \mathbf{u}_N(\mathbf{x}_a)] \, \sin \omega_N t \tag{93}$$

Finally, the mass ratios of the resonators to the entire sphere are defined by

$$\eta_b \equiv \frac{M_b}{\mathcal{M}} \, , \qquad b = 1, \ldots, J \tag{94}$$

and will be *small parameters* in a real device.

Before proceeding further, let us briefly pause for a qualitative inspection of equations (92). Equation (92.a) shows that the sphere's surface deformations $u_a(t)$ are made up of two contributions: one due to the action of *external* agents (GWs or other), contained in $u_a^{\text{external}}(t)$, and another one due to coupling to the resonators. The latter is commanded by the small parameters η_b, and correlates to *all* of the sphere's spheroidal eigenmodes through the kernel matrix $K_{ab}(t)$. This has consequences for GW detectors, for even though GWs may only couple to quadrupole and monopole[14] spheroidal modes of the *free* sphere [37, 9], attachment of resonators causes, as we see, coupling between these and the *other* modes of the antenna; conversely, the latter back-act on the former, too. As I shall shortly prove, such undesirable effects can be minimised by suitably *tuning* the resonators' frequencies.

3.1 Laplace transform domain equations

A solution to equations (92) will now be attempted. Equation (92.a) is an integral equation belonging in the general class of Volterra equations [59], but the usual iterative solution to it by repeated substitution of $u_b(t)$ into the kernel integral is not viable here due to the *dynamical* contribution of $z_b(t)$, which is in turn governed by the *differential* equation (92.b).

A better suited method to solve this *integro-differential* system is to Laplace-transform it. I denote the Laplace transform of a generic function of time $f(t)$ with a *caret* ($\hat{}$) on its symbol, e.g.,

$$\hat{f}(s) \equiv \int_0^\infty f(t) \, e^{-st} \, dt \tag{95}$$

and make the assumption that the system is at rest before an instant of time, $t = 0$, say, or

$$\mathbf{u}(\mathbf{x}, 0) = \dot{\mathbf{u}}(\mathbf{x}, 0) = z_a(0) = \dot{z}_a(0) = 0 \tag{96}$$

Equations (92) then adopt the equivalent form

$$\hat{u}_a(s) \;=\; \hat{u}_a^{\text{external}}(s) - \sum_{b=1}^{J} \eta_b \, \hat{K}_{ab}(s) \, [\hat{z}_b(s) - \hat{u}_b(s)] \tag{97.a}$$

$$s^2 \, \hat{z}_a(s) \;=\; \hat{\xi}_a^{\text{external}}(s) - \Omega_a^2 \, [\hat{z}_a(s) - \hat{u}_a(s)] \, , \qquad a = 1, \ldots, J \tag{97.b}$$

for which use has been made of the *convolution theorem* for Laplace transforms[15]. A further simplification is accomplished if we consider that we shall in practice be only concerned with the *measurable* quantities

[13] The capitalised index N will often be used to imply the multiple index $\{nlm\}$ which characterises the sphere's wave-functions.

[14] Monopole modes only exist in scalar-tensor theories of gravity, such as e.g. Brans–Dicke [11]; General Relativity of course does not belong in this category.

[15] This theorem states, it is recalled, that the Laplace transform of the convolution product of two functions is the arithmetic product of their respective Laplace transforms.

$$q_a(t) \equiv z_a(t) - u_a(t) \ , \qquad a = 1, \ldots, J \tag{98}$$

representing the resonators' actual elastic deformations —cf. Figure 2. It is readily seen that these verify the following:

$$\sum_{b=1}^{J} \left[\delta_{ab} + \eta_b \, \frac{s^2}{s^2 + \Omega_a^2} \, \hat{K}_{ab}(s) \right] \hat{q}_b(s) = - \frac{s^2}{s^2 + \Omega_a^2} \, \hat{u}_a^{\text{external}}(s) + \frac{\hat{\xi}_a^{\text{external}}(s)}{s^2 + \Omega_a^2} \ , \qquad a = 1, \ldots, J \tag{99}$$

Equations (99) constitute a significant simplification of the original problem, as they are a set of just J *algebraic* rather than integral or differential equations. We must solve them for the unknowns $\hat{q}_a(s)$, then perform *inverse Laplace transforms* to revert to $q_a(t)$. I come to this next.

4 System response to a Gravitational Wave

Our concern now is the actual system response when it is acted upon by an incoming GW. It will be calculated by making a number of simplifying assumptions, more precisely:

i) The detector is perfectly spherical.

ii) The resonators have identical masses and resonance frequencies.

iii) The resonators' frequency is accurately matched to one of the sphere's oscillation eigenfrequencies.

It will be shown below (section 7) that a real system can be appropriately treated as one which deviates by definite amounts from this idealised construct. Therefore detailed knowledge of the ideal system behaviour is essential for all purposes: such is the justification for the above simplifications.

The wave-functions $\mathbf{u}_{nlm}(\mathbf{x})$ of an elastic sphere can be found in reference [37] in full detail, and I shall keep the notation of that paper for them. The Laplace transform of the kernel matrix (93) can thus be expressed as —see equation (158) in appendix A.1:

$$\hat{K}_{ab}(s) = \sum_{nl} \frac{\Omega_b^2}{s^2 + \omega_{nl}^2} \, |A_{nl}(R)|^2 \, \frac{2l+1}{4\pi} \, P_l(\mathbf{n}_a \cdot \mathbf{n}_b) \equiv \sum_{nl} \frac{\Omega_b^2}{s^2 + \omega_{nl}^2} \, \chi_{ab}^{(nl)} \tag{100}$$

where the last term simply *defines* the quantities $\chi_{ab}^{(nl)}$. Note that the sums here extend over the *entire* spectrum of the solid sphere.

The assumption that all the resonators are *identical* simply means that

$$\eta_1 = \ldots = \eta_J \equiv \eta \ , \qquad \Omega_1 = \ldots = \Omega_J \equiv \Omega \tag{101}$$

The third hypothesis makes reference to the fundamental idea behind using resonators, which is to have them tuned to one of the frequencies of the sphere's spectrum. This is expressed by

$$\Omega = \omega_{n_0 l_0} \tag{102}$$

where $\omega_{n_0 l_0}$ is a specific and *fixed* frequency of the spheroidal spectrum.

In a GW detector it will only make sense to choose $l_0 = 0$ or $l_0 = 2$, as only monopole and quadrupole sphere modes couple to the incoming signal; in practice, n_0 will refer to the first, or perhaps second harmonic [13]. I shall however keep the generic expression (102) for the time being in order to encompass all the possibilities with a unified notation.

Based on the above hypotheses, equation (99) can be rewritten in the form

$$\sum_{b=1}^{J}\left[\delta_{ab}+\eta\sum_{nl}\frac{\Omega^2 s^2}{(s^2+\Omega^2)(s^2+\omega_{nl}^2)}\,\chi_{ab}^{(nl)}\right]\hat{q}_b(s)=-\frac{s^2}{s^2+\Omega^2}\,\hat{u}_a^{\rm GW}(s)+\frac{\hat{\xi}_a^{\rm GW}(s)}{s^2+\Omega^2}\ ,\qquad(\Omega=\omega_{n_0l_0})\tag{103}$$

where $\hat{\xi}_a^{\rm GW}(s)$ is the Laplace transform of (88), i.e.,

$$\hat{\xi}_a^{\rm GW}(s)=R\sum_{\substack{l=0\ \text{and}\ 2\\ m=-l,\ldots,l}}Y_{lm}(\mathbf{n}_a)\,\hat{g}^{(lm)}(s)\ ,\qquad a=1,\ldots,J\tag{104}$$

As mentioned at the end of the previous section, the matrix in the lhs of (103) must now be inverted; this will give us an expression for $\hat{q}_a(s)$, whose *inverse Laplace transform* will take us back to the time domain. A simple glance at the equation suffices however to grasp the unsurmountable difficulties of accomplishing this *analytically*.

Thankfully, though, a *perturbative* approach is applicable when the masses of the resonators are small compared to the mass of the whole sphere, i.e., when the inequality

$$\eta\ll 1\tag{105}$$

holds. I shall henceforth assume that this is the case, as also is with cylindrical bar resonant transducers. It is shown in appendix A.2 that the perturbative series happens in ascending powers of $\eta^{1/2}$, rather than η itself, and that the lowest order contribution has the form

$$\hat{q}_a(s)=\eta^{-1/2}\sum_{l,m}\hat{\Lambda}_a^{(lm)}(s;\Omega)\,\hat{g}^{(lm)}(s)+O(0)\ ,\qquad a=1,\ldots,J\tag{106}$$

where $O(0)$ stands for terms of order η^0 or smaller. Here, $\hat{\Lambda}_a^{(lm)}(s;\Omega)$ is a *transfer function matrix* which relates *linearly* the system response $\hat{q}_a(s)$ to the GW amplitudes $\hat{g}^{(lm)}(s)$, in the usual sense that $q_a(t)$ is given by the *convolution product* of the signal $g^{(lm)}(t)$ with the time domain expression, $\Lambda_a^{(lm)}(t;\Omega)$, of $\hat{\Lambda}_a^{(lm)}(s;\Omega)$. The detector is thus seen to act as a *linear filter* on the GW signal, whose frequency response is characterised by the properties of $\hat{\Lambda}_a^{(lm)}(s;\Omega)$. More specifically, the filter has a number of characteristic frequencies which correspond to the *imaginary parts of the poles* of $\hat{\Lambda}_a^{(lm)}(s;\Omega)$. As also shown in appendix A.2, these frequencies are the symmetric pairs

$$\omega_{a\pm}^2=\Omega^2\left(1\pm\sqrt{\frac{2l+1}{4\pi}}\,|A_{n_0l_0}(R)|\,\zeta_a\,\eta^{1/2}\right)+O(\eta)\ ,\qquad a=1,\ldots,J\tag{107}$$

where ζ_a^2 is the a-th eigenvalue of the Legendre matrix

$$P_{l_0}(\mathbf{n}_a\cdot\mathbf{n}_b)\ ,\qquad a,b=1,\ldots,J\tag{108}$$

associated to the multipole (l_0) selected for tuning —see (102). These frequency pairs correspond to *beats*, typical of resonantly coupled oscillating systems —we shall find them again in section 6 in a particularly illuminating example.

Equation (106) neatly displays the amplification coefficient $\eta^{-1/2}$ of the resonators' motion amplitudes, which corresponds to the familiar resonant energy transfer in coupled systems of linear oscillators [4].

The specific form of the transfer function matrix $\hat{\Lambda}_a^{(lm)}(s;\Omega)$ depends both on the selected mode to tune the resonator frequency Ω and on the resonator distribution geometry. I now come to a discussion of these.

4.1 Monopole gravitational radiation sensing

General Relativity, as is well known, forbids monopole GW radiation. More general *metric* theories, e.g. Brans-Dicke [11], do however predict this kind of radiation. It appears that a spherical antenna is potentially sensitive to monopole waves, so it can serve the purpose of thresholding, or eventually detecting them. It is therefore relevant to consider the system response to scalar waves.

This clearly requires that the resonator set be tuned to a monopole harmonic of the sphere, i.e.,

$$\Omega = \omega_{n0} \ , \qquad (l_0 = 0) \tag{109}$$

where n tags the chosen harmonic —most likely the first ($n=1$) in a thinkable device.

Since $P_0(z) \equiv 1$ (for all z) the eigenvalues of $P_0(\mathbf{n}_a \cdot \mathbf{n}_b)$ are, clearly,

$$\zeta_1^2 = J \ , \qquad \zeta_2^2 = \ \ldots \ = \zeta_J^2 = 0 \tag{110}$$

for *any resonator distribution*. The tuned mode frequency thus splits into a *single* strongly coupled pair:

$$\omega_\pm^2 = \Omega^2 \left(1 \pm \sqrt{\frac{J}{4\pi}} \, |A_{n0}(R)| \, \eta^{1/2} \right) + O(\eta) \ , \qquad \Omega = \omega_{n0} \tag{111}$$

The Λ-matrix of equation (106) is seen to be in this case

$$\hat{\Lambda}_a^{(lm)}(s;\omega_{n0}) = (-1)^J \, \frac{a_{n0}}{\sqrt{J}} \, \frac{1}{2} \, \left[\left(s^2 + \omega_+^2 \right)^{-1} - \left(s^2 + \omega_-^2 \right)^{-1} \right] \, \delta_{l0} \, \delta_{m0} \tag{112}$$

whence the system response is

$$\hat{q}_a(s) = \eta^{-1/2} \, \frac{(-1)^J}{\sqrt{J}} \, a_{n0} \, \frac{1}{2} \, \left[\left(s^2 + \omega_+^2 \right)^{-1} - \left(s^2 + \omega_-^2 \right)^{-1} \right] \, \hat{g}^{(00)}(s) + O(0) \ , \qquad a = 1, \ldots, J \tag{113}$$

regardless of resonator positions. The overlap coefficient a_{n0} is given by (24.a), and can be calculated by means of numerical computer programmes. By way of example, $a_{10}/R = 0.214$, and $a_{20}/R = -0.038$ for the first two harmonics.

A few interesting facts are displayed by equation (113). First, as already stressed, it is seen that if the resonators are tuned to a monopole *detector* frequency then only monopole *wave amplitudes* couple strongly to the system, even if quadrupole radiation amplitudes are significantly high at the observation frequencies $\omega_\pm$. Also, the amplitudes $\hat{q}_a(s)$ are equal for all a, as corresponds to the spherical symmetry of monopole sphere's oscillations, and are proportional to $J^{-1/2}$, a factor we should indeed expect as an indication that GW *energy* is evenly distributed amongst all the resonators. A *single* transducer suffices to experimentally determine the only monopole GW amplitude $\hat{g}^{(00)}(s)$, of course, but (113) provides the system response if more than one sensor is mounted on the antenna for whatever reasons.

4.2 Quadrupole gravitational radiation sensing

I now consider the more interesting case of quadrupole motion sensing. The choice is now, clearly,

$$\Omega = \omega_{n2} \ , \qquad (l_0 = 2) \tag{114}$$

where n labels the chosen harmonic —most likely the first ($n=1$) or the second ($n=2$) in a practical system. The evaluation of the Λ-matrix is now considerably more involved [57], yet a remarkably elegant form is found for it:

$$\hat{\Lambda}_a^{(lm)}(s;\omega_{n2}) = (-1)^N \sqrt{\frac{4\pi}{5}}\, a_{n2} \sum_{b=1}^{J} \left\{ \sum_{\zeta_c \neq 0} \frac{1}{2} \left[\left(s^2+\omega_{c+}^2\right)^{-1} - \left(s^2+\omega_{c-}^2\right)^{-1} \right] \frac{v_a^{(c)} v_b^{(c)*}}{\zeta_c} \right\} Y_{2m}(\mathbf{n}_b)\, \delta_{l2} \tag{115}$$

where $v_a^{(c)}$ is the c-th normalised eigenvector of $P_2(\mathbf{n}_a{\cdot}\mathbf{n}_b)$, associated to the *non-null* eigenvalue ζ_c^2. Let me stress that equation (115) explicitly shows that at most 5 pairs of modes, of frequencies $\omega_{c\pm}$, couple strongly to quadrupole GW amplitudes, *no matter how many resonators in excess of 5 are mounted on the sphere*. The tidal overlap coefficients a_{2n} can also be calculated using (24.b), and give for the first two harmonics

$$\frac{a_{12}}{R} = 0.328 \ , \qquad \frac{a_{22}}{R} = 0.106 \tag{116}$$

The system response is thus

$$\begin{aligned} \hat{q}_a(s) \ &= \ \eta^{-1/2}\,(-1)^J \sqrt{\frac{4\pi}{5}}\, a_{n2} \sum_{b=1}^{J} \left\{ \sum_{\zeta_c \neq 0} \frac{1}{2} \left[\left(s^2+\omega_{c+}^2\right)^{-1} - \left(s^2+\omega_{c-}^2\right)^{-1} \right] \frac{v_a^{(c)} v_b^{(c)*}}{\zeta_c} \right\} \times \\ &\times \sum_{m=-2}^{2} Y_{2m}(\mathbf{n}_b)\, \hat{g}^{(2m)}(s) + O(0) \ , \qquad a = 1 \ldots, J \end{aligned} \tag{117}$$

Equation (117) is *completely general*, i.e., it is valid for any resonator configuration over the sphere's surface, and for any number of resonators. It describes precisely how all 5 GW amplitudes $\hat{g}^{(2m)}(s)$ interact with all 5 strongly coupled system modes; like before, *only quadrupole wave amplitudes* are seen in the detector (to leading order) when $\Omega = \omega_{n2}$, even if the incoming wave carries significant monopole energy at the frequencies $\omega_{c\pm}$.

The degree of generality and algebraic simplicity of (117) is new in the literature. As we shall now see, it makes possible a systematic search for different resonator distributions and their properties.

5 The *PHC* configuration

Merkowitz and Johnson's *TIGA* [30] is highly symmetric, and is the minimal set with maximum degeneracy, i.e., all the non-null eigenvalues ζ_a are equal. To accomplish this, however, 6 rather than 5 resonators are required on the sphere's surface. Since there are just 5 quadrupole GW amplitudes one may wonder whether there are alternative layouts with *only* 5 resonators. Equation (117) is completely general, so it can be searched for an answer to this question. In reference [38] a specific proposal was made, which I now describe in detail.

In pursuing a search for 5 resonator sets I found that distributions having a sphere diameter as an axis of *pentagonal symmetry*[16] exhibit a rather appealing structure. More specifically, let the resonators be located at the spherical positions

$$\theta_a = \alpha \qquad (\text{all } a) \ , \qquad \varphi_a = (a-1)\,\frac{2\pi}{5} \ , \qquad a = 1, \ldots, 5 \tag{118}$$

The eigenvalues and eigenvectors of $P_2(\mathbf{n}_a{\cdot}\mathbf{n}_b)$ are easily calculated:

$$\zeta_0^2 = \tfrac{5}{4}\,\left(3\,\cos^2\alpha - 1\right)^2 \ , \qquad \zeta_1^2 = \zeta_{-1}^2 = \tfrac{15}{2}\,\sin^2\alpha\,\cos^2\alpha \ , \qquad \zeta_2^2 = \zeta_{-2}^2 = \tfrac{15}{8}\,\sin^4\alpha \tag{119.a}$$

$$v_a^{(m)} = \sqrt{\tfrac{4\pi}{5}}\,\zeta_m^{-1}\,Y_{2m}(\mathbf{n}_a) \ , \qquad m = -2, \ldots, 2 \ , \quad a = 1, \ldots, 5 \tag{119.b}$$

[16] By this I mean resonators are placed along a *parallel* of the sphere every 72°.

so the Λ-matrix is also considerably simple in structure in this case:

$$\hat{\Lambda}_a^{(lm)}(s;\omega_{n2}) = -\sqrt{\frac{4\pi}{5}}\, a_{n2}\, \zeta_m^{-1}\, \frac{1}{2}\left[\left(s^2+\omega_{m+}^2\right)^{-1} - \left(s^2+\omega_{m-}^2\right)^{-1}\right] Y_{2m}(\mathbf{n}_a)\, \delta_{l2}\ , \quad PHC \tag{120}$$

where the notation

$$\omega_{m\pm}^2 = \Omega^2\, \left(1 \pm \sqrt{\frac{5}{4\pi}}\ |A_{n2}(R)|\ \zeta_m\, \eta^{1/2}\right) + O(\eta)\ , \qquad m=-2,\ldots,2 \tag{121}$$

has been used. As seen in these formulas, the *five* expected pairs of frequencies actually reduce to *three*, so pentagonal distributions keep a certain degree of degeneracy, too. The most important distinguishing characteristic of the general *pentagonal* layout is best displayed by the explicit system response:

$$\begin{aligned}
\hat{q}_a(s) \;&=\; -\eta^{-1/2}\sqrt{\frac{4\pi}{5}}\, a_{n2} \\
&\times\; \left\{ \frac{1}{2\zeta_0}\left[\left(s^2+\omega_{0+}^2\right)^{-1} - \left(s^2+\omega_{0-}^2\right)^{-1}\right] Y_{20}(\mathbf{n}_a)\, \hat{g}^{(20)}(s) \right. \\
&+\; \frac{1}{2\zeta_1}\left[\left(s^2+\omega_{1+}^2\right)^{-1} - \left(s^2+\omega_{1-}^2\right)^{-1}\right] \left[Y_{21}(\mathbf{n}_a)\, \hat{g}^{(11)}(s) + Y_{2-1}(\mathbf{n}_a)\, \hat{g}^{(1\,-1)}(s)\right] \\
&+\; \left. \frac{1}{2\zeta_2}\left[\left(s^2+\omega_{2+}^2\right)^{-1} - \left(s^2+\omega_{2-}^2\right)^{-1}\right] \left[Y_{22}(\mathbf{n}_a)\, \hat{g}^{(22)}(s) + Y_{2-2}(\mathbf{n}_a)\, \hat{g}^{(2\,-2)}(s)\right] \right\}
\end{aligned} \tag{122}$$

This equation indicates that *different wave amplitudes selectively couple to different detector frequencies*. This should be considered a very remarkable fact, for it thence follows that simple inspection of the system readout *spectrum*[17] immediately reveals whether a given wave amplitude $\hat{g}^{2m}(s)$ is present in the incoming signal or not.

Pentagonal configurations also admit *mode channels*, which are easily constructed from (122) thanks to the orthonormality property of the eigenvectors (119.b):

$$\hat{y}^{(m)}(s) \equiv \sum_{a=1}^{5} v_a^{(m)*}\, \hat{q}_a(s) = \eta^{-1/2}\, a_{n2}\, \frac{1}{2}\left[\left(s^2+\omega_{m+}^2\right)^{-1} - \left(s^2+\omega_{m-}^2\right)^{-1}\right] \hat{g}^{(2m)}(s) + O(0) \tag{123}$$

These are almost identical to the *TIGA* mode channels [46], the only difference being that each mode channel comes now at a *single specific* frequency pair $\omega_{m\pm}$.

Mode channels are fundamental in signal deconvolution algorithms in noisy systems [49, 51]. Pentagonal resonator configurations should thus be considered non-trivial candidates for a real GW detector.

Based on these facts one may next ask which is a suitable transducer distribution with an axis of pentagonal symmetry. Figure 2 shows a plot of the eigenvalues (119.a) as functions of α, the angular distance of the resonator set from the symmetry axis. Several criteria may be adopted to select a specific choice in view of this graph. An interesting one can be arrived at by the following argument. If for ease of mounting, stability, etc., it is desirable to have the detector milled into a close-to-spherical *polyhedric* shape[18] then polyhedra with axes of pentagonal symmetry must be searched. The number of quasi regular *convex* polyhedra is of course finite —there actually are only 18 of them [28, 25]—, and I found a particularly appealing one in the so called *pentagonal hexacontahedron* (*PHC*), displayed in Figure 3, left —see also [38]. This is a 60 face polyhedron, whose faces are the identical *irregular pentagons* of Figure 3, right. The *PHC* admits an *inscribed sphere* which is tangent to each face at the

[17] In a noiseless system, of course.

[18] This is the philosophy suggested and experimentally implemented by Merkowitz and Johnson at *LSU*.

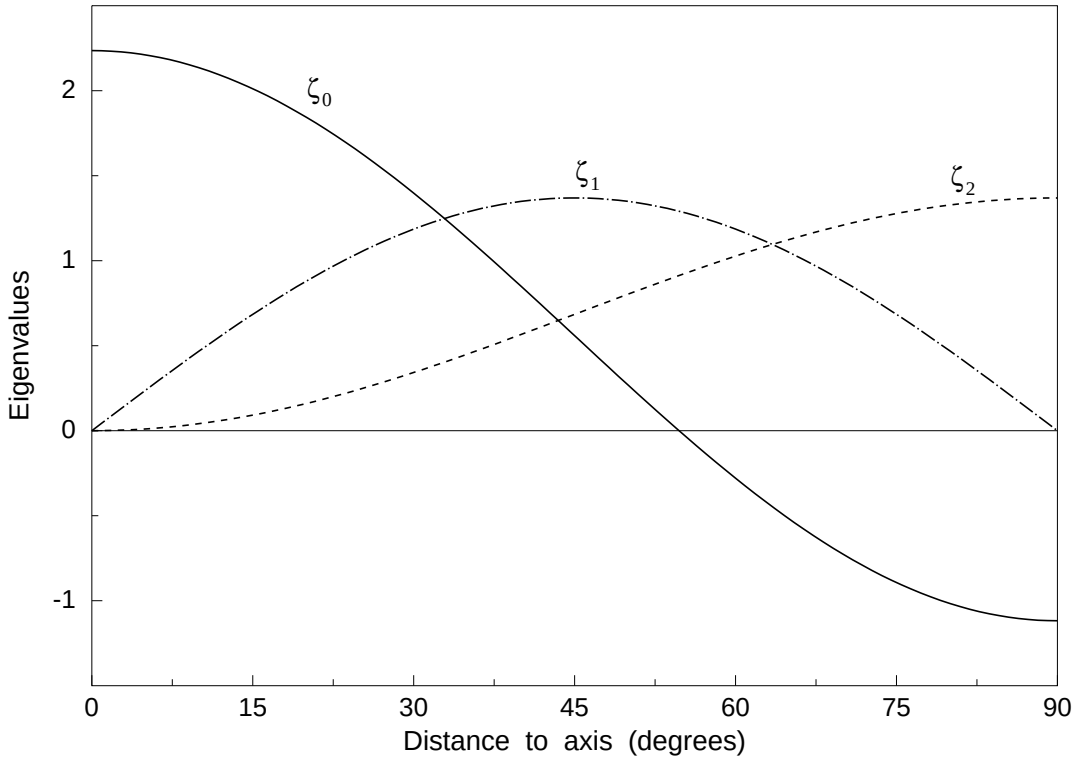

Figure 2: The three distinct eigenvalues ζ_m $(m=0,1,2)$ as functions of the distance of the resonator parallel's co-latitude α relative to the axis of symmetry of the distribution, cf. equation (119.a).

central point marked in the Figure. It is clearly to this point that a resonator should be attached so as to simulate an as perfect as possible spherical distribution.

The *PHC* is considerably spherical: the ratio of its volume to that of the inscribed sphere is 1.057, which quite favourably compares to the value of 1.153 for the ratio of the circumscribed sphere to the TI volume. If the frequency pairs $\omega_{m\pm}$ are now requested to be as *evenly spaced* as possible, compatible with the *PHC* face orientations, then the choice $\alpha = 67.617^\circ$ is unambiguously singled out. Hence

$$\omega_{0\pm} = \omega_{12}\left(1 \pm 0.5756\,\eta^{1/2}\right)\ , \quad \omega_{1\pm} = \omega_{12}\left(1 \pm 0.8787\,\eta^{1/2}\right)\ , \quad \omega_{2\pm} = \omega_{12}\left(1 \pm 1.0668\,\eta^{1/2}\right) \quad (124)$$

for instance for $\Omega = \omega_{12}$, the first quadrupole harmonic. Figure 4 shows this frequency spectrum together with the multiply degenerate *TIGA* for comparison.

The criterion leading to the *PHC* proposal is of course not unique, and alternatives can be considered. For example, if the 5 faces of a regular icosahedron are selected for sensor mounting ($\alpha = 63.45^\circ$) then a four-fold degenerate pair plus a single non-degenerate pair is obtained; if the resonator parallel is 50° or 22.6° away from the "north pole" then the three frequencies ω_{0+}, ω_{1+}, and ω_{2+} are equally spaced; etc. The number of choices is virtually infinite if the sphere is not milled into a polyhedric shape [58, 44].

Let me finally recall that the complete *PHC* proposal [38] was made with the idea of building an as complete as possible spherical GW antenna, which amounts to making it sensitive at the first *two* quadrupole frequencies *and* at the first monopole one. This would take advantage of the good sphere cross section at the second quadrupole harmonic [13], and would enable measuring (or thresholding) eventual monopole GW radiation. Now, the system *pattern matrix* $\hat{\Lambda}_a^{(lm)}(s;\Omega)$ has *identical structure*

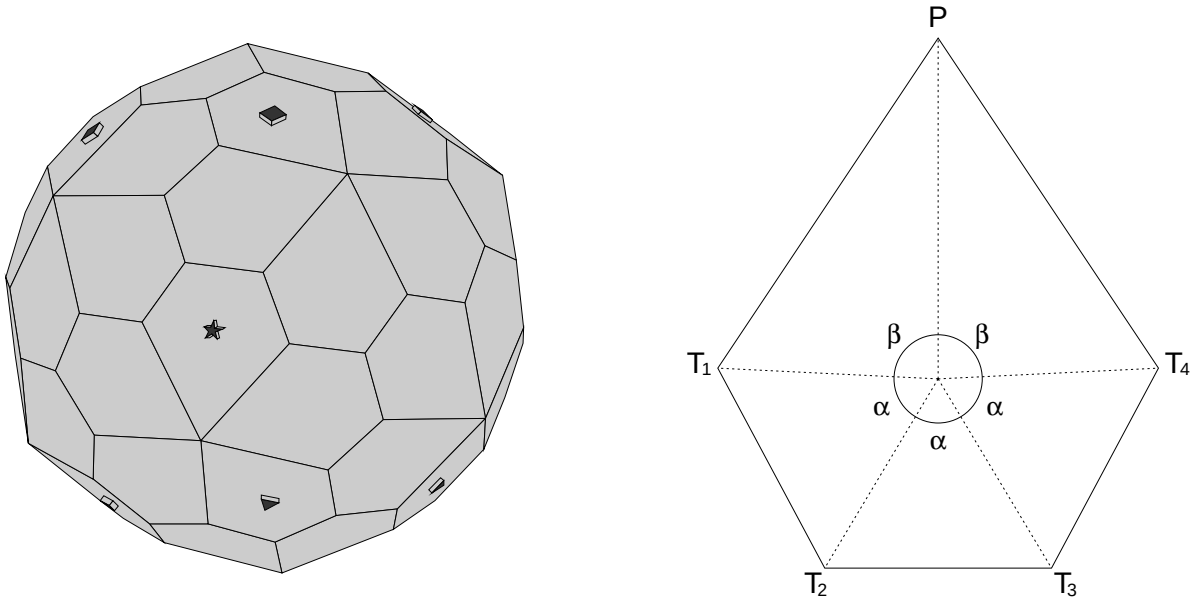

Figure 3: To the left, the *pentagonal hexacontahedron* shape. Certain faces are marked to indicate resonator positions in a specific proposal —see text— as follows: a *square* for resonators tuned to the first quadrupole frequency, a *triangle* for the second, and a *star* for the monopole. On the right we see the (pentagonal) face of the polyhedron. A few details about it: the confluence point of the dotted lines at the centre is the tangency point of the *inscribed* sphere to the *PHC*; the labeled angles have values $\alpha = 61.863°$, $\beta = 87.205°$; the angles at the T-vertices are all equal, and their value is 118.1366°, while the angle at P is 67.4536°; the ratio of a long edge (e.g. PT_1) to a short one (e.g. T_1T_2) is 1.74985, and the radius of the inscribed sphere is *twice* the long edge of the pentagon, $R = 2\,PT_1$.

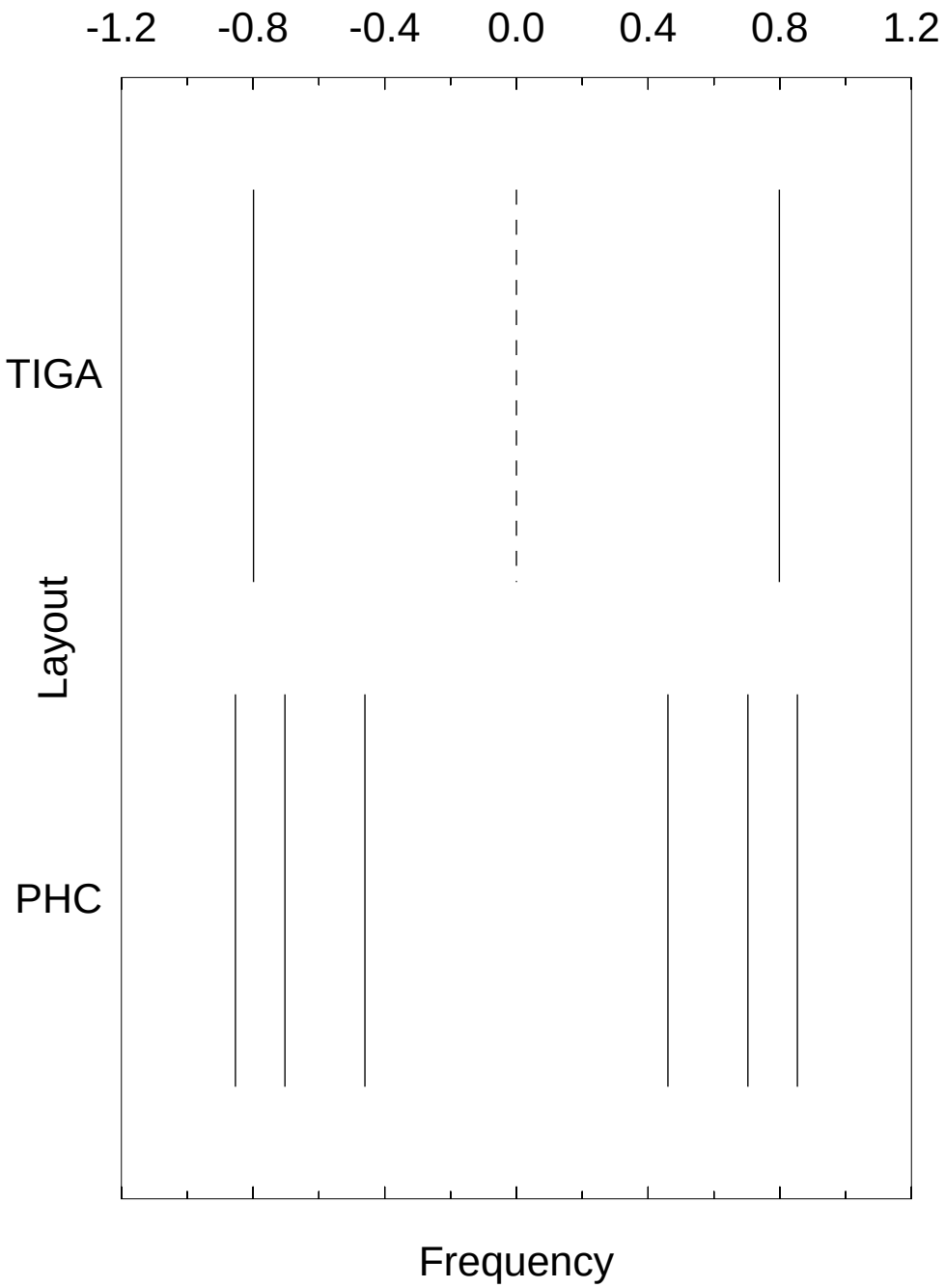

Figure 4: Compared line spectrum of a coupled *TIGA* and a *PHC* resonator layout in an ideally spherical system. The weakly coupled central frequency in the *TIGA* is drawn dashed. The frequency pair is 5-fold degenerate for this layout, while the two outer pairs of the *PHC* are doubly degenerate each, and the inner pair is non-degenerate. Units in abscissas are $\eta^{1/2}\Omega$, and the central value, labeled 0.0, corresponds to Ω.

for all the harmonics of a given l series —see (112) and (115)—, and so too identical criteria for resonator layout design apply to either set of transducers, respectively tuned to ω_{12} and ω_{22}. The *PHC* proposal is best described graphically in Figure 3, left: a *second* set of resonators, tuned to the second quadrupole harmonic ω_{22} can be placed in an equivalent position in the "southern hemisphere", and an eleventh resonator tuned to the first monopole frequency ω_{10} is added at an arbitrary position. It is not difficult to see, by the general methods outlined earlier on in this paper, that cross interaction between these three sets of resonators is only *second order* in $\eta^{1/2}$, therefore weak.

A spherical GW detector with such a set of altogether 11 transducers would be a very complete multi-mode multi-frequency device with an unprecedented capacity as an individual antenna. Amongst other, it would practically enable monitoring of coalescing binary *chirp* signals by means of a rather robust double passage method [15], a prospect which was considered so far possible only with broadband long baseline laser interferometers [18, 31], and is almost unthinkable with currently operating cylindrical bars.

6 A calibration signal: hammer stroke

This section is a brief digression from the main streamline of the paper. I propose to assess now the system response to a particular, but useful, calibration signal: a perpendicular *hammer stroke*.

Let us first go back to equation (99) and replace $\hat{u}_a^{\text{external}}(s)$ in its rhs with that corresponding to a hammer stroke, which is easily calculated —cf. appendix A.1:

$$\hat{u}_a^{\text{stroke}}(s) = -\sum_{nl} \frac{f_0}{s^2+\omega_{nl}^2}\, |A_{nl}(R)|^2\, P_l(\mathbf{n}_a\cdot\mathbf{n}_0)\ , \qquad a=1,\ldots,J \tag{125}$$

where $\mathbf{n}_0$ are the spherical coordinates of the hit point on the sphere, and $f_0 \equiv \mathbf{n}_0\cdot\mathbf{f}_0/\mathcal{M}$. Clearly, the hammer stroke excites *all* of the sphere's vibration eigenmodes, as it has a completly flat spectrum.

The coupled system resonances are again those calculated in appendix A.2. The same procedures described in section 4 for a GW excitation can now be pursued to obtain

$$\begin{aligned}\hat{q}_a(s) \;&=\; \eta^{-1/2}\,(-1)^{J-1}\sqrt{\frac{2l+1}{4\pi}}\,f_0\,|A_{nl}(R)|\,\times \\ &\times\; \sum_{b=1}^{J}\left\{\sum_{\zeta_c\neq 0}\frac{1}{2}\left[\left(s^2+\omega_{c+}^2\right)^{-1}-\left(s^2+\omega_{c-}^2\right)^{-1}\right]\frac{v_a^{(c)}v_b^{(c)*}}{\zeta_c}\right\}P_l(\mathbf{n}_b\cdot\mathbf{n}_0)+O(0)\end{aligned} \tag{126}$$

where $a=1,\ldots,J$, when the system is tuned to the nl-th spheroidal harmonic, i.e., $\Omega=\omega_{nl}$. It is immediately seen from here that the system response to this signal when the resonators are tuned to a *monopole* frequency is given by

$$\hat{q}_a(s) = \eta^{-1/2}\,(-1)^{J-1}\,\frac{f_0}{\sqrt{4\pi J}}\,|A_{n0}(R)|\,\frac{1}{2}\left[\left(s^2+\omega_+^2\right)^{-1}-\left(s^2+\omega_-^2\right)^{-1}\right]\ , \qquad \Omega=\omega_{n0} \tag{127}$$

an expression which holds for all a, and is independent of either the resonator layout or the hit point, which in particular prevents any determination of the latter, as obviously expected. The frequencies $\omega_\pm$ are those of (111), and we find here again a global factor $J^{-1/2}$, as also expected.

Consider next the situation when quadrupole tuning is implemented, $\Omega=\omega_{n2}$. Only the *PHC* and *TIGA* configurations will be addressed, as more general cases are not quite as interesting at this point.

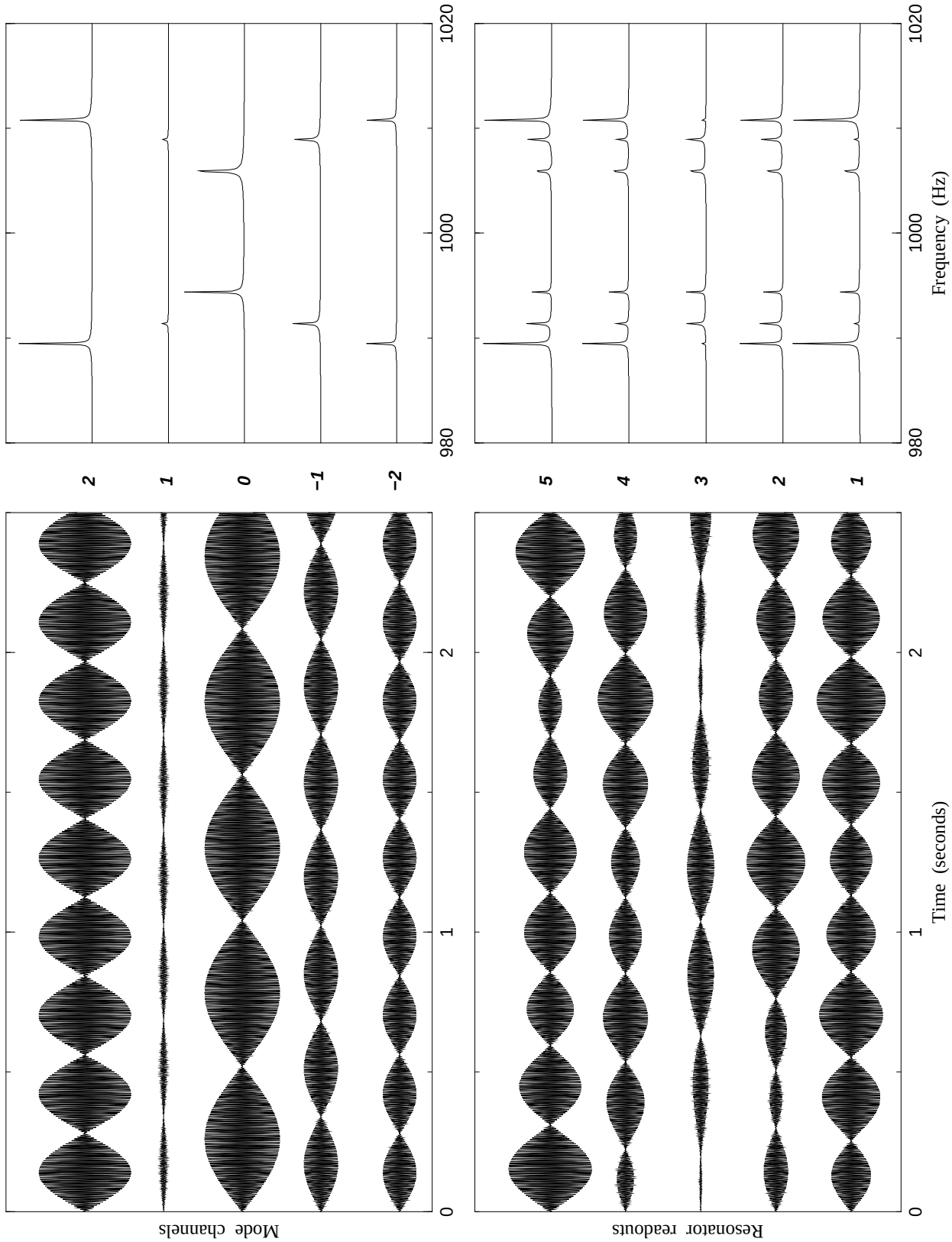

Figure 5: Simulated response of a *PHC* to a hammer stroke: the time series and their respective spectra, both for direct resonator readouts and mode channels. Note that while the former are *not* simple beats, the latter are.

6.1 *PHC* and *TIGA* response to a hammer stroke

Expanding equation (126) by substitution of the eigenvalues ζ_m and eigenvectors $v_a^{(m)}$ of the *PHC*, one readily finds that the system response is given by

$$\hat{q}_a(s) = \eta^{-1/2}\, f_0 \sqrt{\frac{4\pi}{5}}\, |A_{n2}(R)| \sum_{m=-2}^{2} \frac{1}{2}\left[\left(s^2+\omega_{m+}^2\right)^{-1} - \left(s^2+\omega_{m-}^2\right)^{-1}\right] \zeta_m^{-1}\, Y_{2m}(\mathbf{n}_a)\, Y_{2m}^*(\mathbf{n}_0) \quad (128)$$

with $a = 1, \ldots, 5$, and the mode channels by

$$\hat{y}^{(m)}(s) = \eta^{-1/2}\, f_0\, |A_{n2}(R)|\, \frac{1}{2}\left[\left(s^2+\omega_{m+}^2\right)^{-1} - \left(s^2+\omega_{m-}^2\right)^{-1}\right] Y_{2m}^*(\mathbf{n}_0)\ , \quad m = -2, \ldots, 2 \quad (129)$$

These equations indicate that the system response $q_a(t)$ is a *superposition of three different beats*[19], while the mode channels are *single* beats each, but with *differing modulation frequencies*. This is represented graphically in Figure 5, where we see the result of a numerical simulation of the *PHC* response to a hammer stroke, delivered to the solid at a given location. The readouts $q_a(t)$ are somewhat complex time series, whose frequency spectrum shows *three pairs of peaks* —in fact, the *lines* in the ideal spectrum of Figure 4. The mode channels on the other hand are *pure beats*, whose spectra consist of the *individually separate* pairs of the just mentioned peaks.

The response of the *TIGA* layout to a hammer stroke has been described in detail by Merkowitz and Johnson —see e.g. reference [48]. The present formalism does of course lead to the results obtained by them; in the notation of this paper, we have

$$\hat{q}_a(s) \;=\; -\eta^{-1/2}\, \frac{5}{\sqrt{24\pi}}\, f_0\, |A_{n2}(R)|\, \frac{1}{2}\left[\left(s^2+\omega_{+}^2\right)^{-1} - \left(s^2+\omega_{-}^2\right)^{-1}\right] P_2(\mathbf{n}_a\cdot\mathbf{n}_0) \quad (130.a)$$

$$\hat{y}^{(m)}(s) \;=\; -\eta^{-1/2}\, f_0\, |A_{n2}(R)|\, \frac{1}{2}\left[\left(s^2+\omega_{+}^2\right)^{-1} - \left(s^2+\omega_{-}^2\right)^{-1}\right] Y_{2m}^*(\mathbf{n}_0)\ , \quad m = -2, ..., 2 \quad (130.b)$$

for the system response and the mode channels, respectively, where

$$\omega_{\pm}^2 = \omega_{n2}^2 \left(1 \pm \sqrt{\frac{3}{2\pi}}\, |A_{n2}(R)|\, \eta^{1/2}\right) + O(\eta)\ , \qquad a = 1, \ldots, 6 \quad (131)$$

are the five-fold degenerate frequency pairs corresponding to the *TIGA* distribution. Comparison of the mode channels shows that they are identical for *PHC* and *TIGA*, except that the former come at different frequencies depending on the index m. One might perhaps say that the *PHC* gives rise to a sort of "Zeeman splitting" of the *TIGA* degenerate frequencies, which can be attributed to an *axial symmetry breaking* of that resonator distribution: the *PHC* mode channels partly split up the otherwise degenerate multiplet into its components.

7 Symmetry defects

So far we have made the assumption that the sphere is perfectly symmetric, that the resonators are identical, that their locations on the sphere's surface are ideally accurate, etc. This is of course unrealistic. So I propose to address now how departures from such ideal conditions affect the system

[19] A *beat* is a modulated oscillation of the form $\sin\frac{1}{2}(\omega_+ - \omega_-)t\, \cos\Omega t$, where ω_+ and ω_- are nearby frequencies, and $\omega_+ + \omega_- = 2\,\Omega$. The Laplace transform of such function of time is precisely $(\Omega/2)\left[\left(s^2+\omega_+^2\right)^{-1} - \left(s^2+\omega_-^2\right)^{-1}\right]$, up to higher order terms in the difference $\omega_+ - \omega_-$, which in this case is proportional to $\eta^{1/2}$.

behaviour. As we shall see, the system is rather *robust*, in a sense to be made precise shortly, against a number of small defects.

In order to *quantitatively* assess ideality failures I shall adopt a philosophy which is naturally suggested by the results already obtained in an ideal system. It is as follows.

As seen in previous sections, the solution to the general equations (99) must be given as a *perturbative* series expansion in ascending powers of the small quantity $\eta^{1/2}$. This is clearly a fact *not* related to the system's symmetries, so it will survive symmetry breakings. It is therefore appropriate to *parametrise* deviations from ideality in terms of suitable powers of $\eta^{1/2}$, in order to address them *consistently with the order of accuracy of the series solution to the equations of motion*. An example will better illustrate the situation.

In a *perfectly ideal* spherical detector the system frequencies are given by equations (107). Now, if a small departure from e.g. spherical symmetry is present in the system then we expect that a correspondingly small correction to those equations will be required. Which specific correction to the formula will actually happen can be *qualitatively* assessed by a *consistency* argument: if symmetry defects are of order $\eta^{1/2}$ then equations (107) will be significantly altered in their $\eta^{1/2}$ terms; if on the other hand such defects are of order η or smaller then any modifications to equations (107) will be swallowed into the $O(0)$ terms, and the more important $\eta^{1/2}$ terms will remain unaffected by the symmetry failure. One can say in this case that the system is *robust* against that symmetry breaking.

More generally, this argument can be extended to see that the only system defects standing a chance to have any influences on lowest order ideal system behaviour are defects of order $\eta^{1/2}$ relative to an ideal configuration. Defects of such order are however *not necessarily guaranteed* to be significant, and a specific analysis is required for each concrete parameter in order to see whether or not the system response is *robust* against the considered parameter deviations. Let us now go into the quantitative detail.

Let P be one of the system parameters, e.g. a sphere frequency, or a resonator mass or location, etc. Let $P_{\rm ideal}$ be the *numerical value* this parameter has in an ideal detector, and let $P_{\rm real}$ be its value in the real case. These two will be assumed to differ by terms of order $\eta^{1/2}$, i.e.,

$$P_{\rm real} = P_{\rm ideal}\,(1 + p\,\eta^{1/2}) \tag{132}$$

For a given system, p is readily determined adopting (132) as the *definition* of $P_{\rm real}$, once a suitable *hypothesis* has been made as to which is the value of $P_{\rm ideal}$. In order for the following procedure to make sensible sense it is clearly required that p be of order 1 or, at least, appreciably larger than $\eta^{1/2}$. Should p thus calculated from (132) happen to be too small, i.e., of order $\eta^{1/2}$ itself or smaller, then the system will be considered *robust* as regards the affected parameter.

7.1 The suspended sphere

An earth based observatory obviously requires a *suspension mechanism* for the large sphere. If a *nodal point* suspension is e.g. selected then a diametral *bore* has to be drilled across the sphere [45]. The most immediate consequence of this is that spherical symmetry is broken, what in turn results in *degeneracy lifting* of the free spectral frequencies ω_{nl}, which now *split* up into multiplets ω_{nlm} ($m = -l,...,l$). The resonators' frequency Ω *cannot* therefore be matched to *the* frequency $\omega_{n_0 l_0}$, but at most to *one* of the $\omega_{n_0 l_0 m}$'s. In this subsection I keep the hypothesis —to be relaxed later, see below— that all the resonators are identical, and assume that Ω falls *within* the span of the multiplet of the $\omega_{n_0 l_0 m}$'s. Then

$$\omega^2_{n_0 l_0 m} = \Omega^2\,(1 + p_m\,\eta^{1/2})\ , \qquad m = -l_0, \ldots, l_0 \tag{133}$$

The coupled frequencies, i.e., the roots of equation (166), will now be searched. The kernel matrix $\hat{K}_{ab}(s)$ is however no longer given by (100), due the removed degeneracy of ω_{nl}, and we must stick to its general expression (155), or

$$\hat{K}_{ab}(s) = \sum_{nlm} \frac{\Omega_b^2}{s^2+\omega_{nlm}^2} \, |A_{nl}(R)|^2 \, \frac{2l+1}{4\pi} \, Y_{lm}^*(\mathbf{n}_a) \, Y_{lm}(\mathbf{n}_b) \equiv \sum_{nlm} \frac{\Omega_b^2}{s^2+\omega_{nlm}^2} \, \chi_{ab}^{(nlm)} \tag{134}$$

Following the steps of appendix A.1 we now seek the roots of the equation

$$\det \left[\delta_{ab} + \eta \sum_{m=-l_0}^{l_0} \frac{\Omega^2 s^2}{(s^2+\Omega^2)(s^2+\omega_{n_0 l_0 m}^2)} \, \chi_{ab}^{(n_0 l_0 m)} + \eta \sum_{nl \neq n_0 l_0, m} \frac{\Omega^2 s^2}{(s^2+\Omega^2)(s^2+\omega_{nlm}^2)} \, \chi_{ab}^{(nlm)} \right] = 0 \tag{135}$$

Since Ω relates to $\omega_{n_0 l_0 m}$ through equation (133) we see that the roots of (135) fall again into either of the two categories (169) (see Appendix A.2), i.e., roots close to $\pm i\Omega$ and roots close to $\pm i\omega_{nlm}$ ($nl \neq n_0 l_0$). I shall exclusively concentrate on the former now. Direct substitution of the series (169.a) into (135) yields the following equation for the coefficient $\chi_{\frac{1}{2}}$:

$$\det \left[\delta_{ab} - \frac{1}{\chi_{\frac{1}{2}}} \sum_{m=-l_0}^{l_0} \frac{\chi_{ab}^{(n_0 l_0 m)}}{\chi_{\frac{1}{2}} - p_m} \right] = 0 \tag{136}$$

This is a variation of (170), to which it reduces when $p_m = 0$, i.e., when there is full degeneracy.

The solutions to (136) no longer come in symmetric pairs, like (107). Rather, there are $2l_0{+}1{+}J$ of them, with a *maximum* number of $2(2l_0{+}1)$ non-identically zero roots if $J \geq 2l_0{+}1$[20]. For example, if we choose to select the resonators' frequency close to a quadrupole multiplet ($l_0 = 2$) then (136) has at most $5{+}J$ non-null roots, *with a maximum ten* no matter how many resonators in excess of 5 we attach to the sphere. Modes associated to null roots of (136) can be seen to be *weakly coupled*, just like in a free sphere, i.e., their amplitudes are smaller than those of the strongly coupled ones by factors of order $\eta^{1/2}$.

In order to assess the reliability of this method I have applied it to see what are its predictions for a *real system*. To this end, data taken with the *TIGA* prototype at *LSU*[21] were used to confront with. The *TIGA* was drilled and suspended from the centre, so its first quadrupole frequency split up into a multiplet of five frequencies. Their reportedly measured values are

$$\omega_{120} = 3249 \text{ Hz} \, , \quad \omega_{121} = 3238 \text{ Hz} \, , \quad \omega_{12\,-1} = 3236 \text{ Hz} \, , \quad \omega_{122} = 3224 \text{ Hz} \, , \quad \omega_{12\,-2} = 3223 \text{ Hz} \, , \tag{137}$$

All 6 resonators were equal, and had the following characteristic frequency and mass, respectively:

$$\Omega = 3241 \text{ Hz} \, , \qquad \eta = \frac{1}{1762.45} \tag{138}$$

Substituting these values into (133) it is seen that

$$p_0 = 0.2075 \, , \quad p_1 = -0.0777 \, , \quad p_{-1} = -0.1036 \, , \quad p_2 = -0.4393 \, , \quad p_{-2} = -0.4650 \tag{139}$$

Equation (136) can now be readily solved, once the resonator positions are fed into the matrices $\chi_{ab}^{(12m)}$. Such positions correspond to the pentagonal faces of a truncated icosahedron. Merkowitz [45] gives a complete account of all the measured system frequencies as resonators are progressively attached to the selected faces, beginning with one and ending with six. Figure 6 graphically displays the experimentally reported frequencies along with those calculated theoretically by solving equation (136). In Table 1 I give the numerical values. As can be seen, coincidence between theoretical predictions and

[20] This is a *mathematical fact*, whose proof is relatively cumbersome, and will be omitted here; let me just mention that it has its origin in the linear dependence of more than $2l_0{+}1$ spherical harmonics of order l_0.

[21] These data are contained in reference [45]; I want to thank Stephen Merkowitz for kindly handing them to me.

Table 4: Numerical values of measured and theoretically predicted frequencies (in Hz) for the *TIGA* prototype with varying number of resonators. Relative errors are also shown as parts in 10^4. The *calculated* values of the tuning and free multiplet frequencies are taken *by definition* equal to the measured ones, and quoted in brackets. In square brackets the frequency of the *weakly coupled* sixth mode in the full, 6 resonator *TIGA* layout. These data are plotted in Figure 6.

Descr.	Meas.	Calc.	Difference (parts in 10^4)	Descr.	Meas.	Calc.	Difference (parts in 10^4)
Tuning	3241	(3241)	(0)	4 reson.	3159	3155	−12
No reson.	3223	(3223)	(0)		3160	3156	−11
	3224	(3224)	(0)		3168	3165	−12
	3236	(3236)	(0)		3199	3198	−5
	3238	(3238)	(0)		3236	3236	0
	3249	(3249)	(0)		3285	3286	3
1 reson.	3167	3164	−8		3310	3310	0
	3223	3223	0		3311	3311	0
	3236	3235	−2		3319	3319	0
	3238	3237	−2	5 reson.	3152	3154	8
	3245	3245	0		3160	3156	−14
	3305	3307	6		3163	3162	−3
2 reson.	3160	3156	−13		3169	3167	−8
	3177	3175	−7		3209	3208	−2
	3233	3233	0		3268	3271	10
	3236	3236	0		3304	3310	17
	3240	3240	0		3310	3311	3
	3302	3303	3		3313	3316	10
	3311	3311	0		3319	3321	6
3 reson.	3160	3155	−15	6 reson.	3151	3154	11
	3160	3156	−13		3156	3155	−3
	3191	3190	−2		3162	3162	0
	3236	3235	−2		3167	3162	−14
	3236	3236	0		3170	3168	−7
	3297	3299	8		[3239]	[3241]	[6]
	3310	3311	2		3302	3309	23
	3311	3311	0		3308	3310	6
					3312	3316	12
					3316	3317	2
					3319	3322	10

experimental data is remarkable: the worst error is 0.2%, while for the most part it is below 0.1%. This is a few parts in 10^4, which is precisely the magnitude of η, as specified in equation (138).

Therefore *discrepancies between theoretical predictions and experimental data are exactly as expected*, i.e., of order η. In addition, it is also reported in reference [48] that the 11-th, weakly coupled mode of the *TIGA* (enclosed in square brackets in Table 1) has a practically zero amplitude, again in excellent agreement with the general theoretical predictions about modes beyond the tenth —see paragraph after equation (136).

This is a remarkable result which encouraged a better fit by estimates of *next order* corrections, i.e., χ_1 of (169.a). As it turned out, however, matching between theory and experiment does not consistently improve in the next step. This is not really that surprising, though, as M&J explicitly state [48] that control of the general experimental conditions in which data were obtained had a certain degree of tolerance, and they actually show satisfaction that $\sim$1% coincidence between theory and measurement is comfortably accomplished. But 1% is *two orders of magnitude larger than* η —cf. equation (138)—, so failure to refine our frequency estimates to order η is again fully consistent with the accuracy of available real data.

A word on a technical issue is in order. Merkowitz and Johnson's equations for the *TIGA* [30, 46] are identical to the equations in this paper to lowest order in η. Remarkably, though, their reported theoretical estimates of the system frequencies are not quite as accurate as those in Table 1 [48]. The reason is probably this: in M&J's model these frequencies appear within an algebraic system of $5+J$ linear equations with as many unknowns which has to be solved; here instead the algebraic system has only J equations and unknowns, actually equations (99). This is a very appreciable difference for the range of values of J under consideration. While the roots for the frequencies *mathematically* coincide in both approaches, in actual practice they are *estimated*, generally by means of computer programmes. It is here that problems most likely arise, for the numerical reliability of an algorithm to solve matrix equations normally decreases as the rank of the matrix increases.

7.2 Other mismatched parameters

We now assess the system sensitivity to small mismatches in resonators' masses, locations and frequencies.

7.2.1 Resonator mass mismatches

If the *masses* are slightly non-equal then one can write

$$M_a = \eta\mathcal{M}\left(1 + \mu_a\,\eta^{1/2}\right) , \qquad a = 1, \ldots, J \tag{140}$$

where η can be defined e.g. as the ratio of the *average* resonator mass to the sphere's mass. It is immediately obvious from equation (140) that mass non-uniformities of the resonators only affect the main equations in *second order*, since resonator mass non-uniformities result, as we see, in corrections of order $\eta^{1/2}$ to $\eta^{1/2}$ itself, which is the very parameter of the perturbative expansions. The system is thus clearly *robust* to mismatches in the resonator masses of the type (140).

7.2.2 Errors in resonator locations

The same happens if the *locations* of the resonators have tolerances relative to a *pre-selected* distribution. For let $\mathbf{n}_a$ be a set of resonator locations, for example the *TIGA* or the *PHC* positions, and let $\mathbf{n'}_a$ be the real ones, close to the former:

$$\mathbf{n'}_a = \mathbf{n}_a + \mathbf{v}_a\,\eta^{1/2} , \qquad a = 1, \ldots, J \tag{141}$$

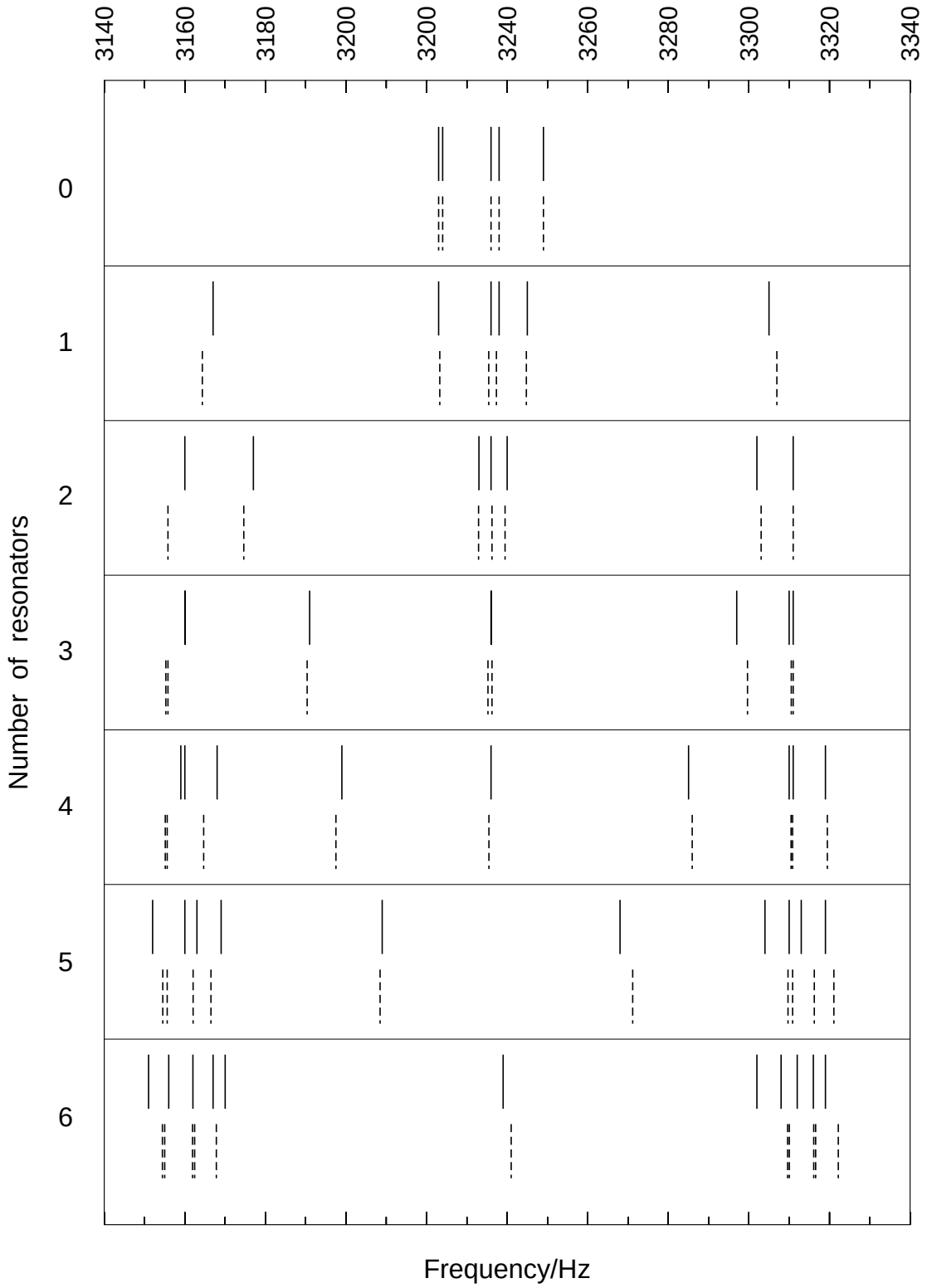

Figure 6: The frequency spectrum of the *TIGA* distribution as resonators are progressively added from none to 6. Continuous lines correspond to measured values, and dashed lines correspond to their $\eta^{1/2}$ theoretical estimates with equation (136).

The values $\mathbf{n}_a$ determine the eigenvalues ζ_a in equation (107), and they also appear as arguments to the spherical harmonics in the system response functions of sections 4–6. It follows from (141) by continuity arguments that

$$Y_{lm}(\mathbf{n'}_a) = Y_{lm}(\mathbf{n}_a) + O(\eta^{1/2}) \tag{142.a}$$
$$\zeta'_a = \zeta_a + O(\eta^{1/2}) \tag{142.b}$$

Inspection of the equations of sections 4–6 shows that both ζ_a and $Y_{lm}(\mathbf{n}_a)$ *always* appear within lowest order terms, and hence that corrections to them of the type (142) will affect those terms in *second order* again. We thus conclude that the system is also *robust* to small misalignments of the resonators relative to pre-established positions.

7.2.3 Resonator frequency mistunings

The resonator *frequencies* may also differ amongst them, so let

$$\Omega_a = \Omega\,(1 + \rho_a\,\eta^{1/2})\ , \qquad a = 1, \ldots, J \tag{143}$$

To assess the consequences of this, however, we must go back to equation (28) and see what the coefficients in its series solutions of the type (169.a) are. The procedure is very similar to that of section 7.1, and will not be repeated here; the lowest order coefficient $\chi_{\frac{1}{2}}$ is seen to satisfy the algebraic equation

$$\det\left[\delta_{ab} - \frac{1}{\chi_{\frac{1}{2}}}\sum_{c=0}^{J}\frac{\chi_{ac}^{(n_0 l_0)}\,\delta_{cb}}{\chi_{\frac{1}{2}} - \rho_c}\right] = 0 \tag{144}$$

which reduces to (170) when all the ρ's vanish, as expected. This appears to potentially have significant effects on our results to lowest order in $\eta^{1/2}$, but a more careful consideration of the facts shows that it is probably unrealistic to think of such large tolerances in resonator manufacturing as implied by equation (143) in the first place. In the *TIGA* experiment, for example [45], an error of order $\eta^{1/2}$ would amount to around 50 Hz of mistuning between resonators, an absurd figure by all means. In a full scale sphere (∼40 tons, ∼3 metres in diameter, ∼800 Hz fundamental quadrupole frequency, $\eta \sim 10^{-5}$) the same error would amount to between 5 Hz and 10 Hz in resonator mistunings for the lowest frequency. This is probably excessive for a capacitive transducer, but may be realistic for an inductive one. With this exception, it is thus more appropriate to consider that resonator mistunings are at least of order η. If this is the case, though, we see once more that the system is quite insensitive to such mistunings.

Summing up the results of this section, one can say that the resonator system dynamics is quite *robust* to small (of order $\eta^{1/2}$) changes in its various parameters. The important exception is of course the effect of suspension drilling, which do result in significant changes relative to the ideally perfect device, but which can be relatively easily calculated. The theoretical picture is fully supported by experiment, as *robustness* in the parameters here considered has been reported in the real device [48].

8 Conclusions

A spherical GW antenna is a natural multi-mode device with very rich potential capabilities to detect GWs on earth. But such detector is not just a bare sphere, it requires a set of *motion sensors* to be practically useful. It appears that transducers of the *resonant* type are the best suited ones for an efficient performance of the detector. Resonators however significantly interact with the sphere, and they affect in particular its frequency spectrum and vibration modes in a specific fashion, which must be properly understood before reliable conclusions can be drawn from the system readout.

The main objective of this paper has been the construction and development of an elaborate theoretical model to describe the joint dynamics of a solid elastic sphere and a set of *radial motion* resonators attached to its surface at arbitrary locations, with the purpose to make predictions of the system characteristics and response, in principle with arbitrary mathematical precision.

The solutions to the equations of motion have been shown to be expressible as an ascending series in powers of the small "coupling constant" η, the ratio of the average resonator mass to the mass of the larger sphere. The *lowest order* approximation corresponds to terms of order $\eta^{1/2}$ and, to this order, previous results [48, 58, 44] are recovered. This, I hope, should contribute to clarify the nature of the approximations inherent in earlier approaches, and to better understand the physical reason for their remarkable accuracy [48].

In addition, the methods of this paper have permitted us to discover that there can be in fact transducer layouts alternative to the highly symmetric *TIGA*, and having potentially interesting practical properties. An example is the *PHC* distribution, which is based on a pentagonally symmetric set of 5 rather than 6 resonators per quadruopole mode sensed. This transducer distribution has the property that *mode channels* can be constructed from the resonators' readouts, much in the same way as in the *TIGA* [46]. In the *PHC* however a new and distinctive characteristic is present: different *wave amplitudes* selectively couple to different *detector modes* having different frequencies, so that the antenna's mode channels come at different rather than equal frequencies. The *PHC* philosophy can be extended to make a *multi-frequency* system by using resonators tuned to the first two quadrupole harmonics of the sphere *and* to the first monopole, an altogether 11 transducer set.

The assessment of *symmetry failure* effects, as well as other parameter departures form ideality, has also been subjected to analysis. The general scheme is again seen to be very well suited for the purpose, as the theory transparently shows that the system is *robust* against relative disturbances of order η or smaller in any system parameters, also providing a systematic procedure to assess larger tolerances —up to order $\eta^{1/2}$. The system is shown to still be robust to tolerances of this order in some of its parameters, whilst it is not to others. Included in the latter group is the effect of spherical symmetry breaking due to system suspension in the laboratory, which causes *degeneracy lifting* of the sphere's eigenfrequencies, which split up into multiplets. A strong point is that, by use of mostly analytic algorithms, it has been possible to accurately reproduce the reportedly measured frequencies of the *LSU* prototype antenna [45] with the predicted precision of four decimal places. The also reported robustness of the system to resonator mislocations [48] is too in satisfactory agreement with the theoretical predictions.

The perturbative approach here adopted is naturally open to refined analysis of the system response in higher orders in η. For example, one can systematically address the weaker coupling of non-quadrupole modes, etc. It appears however that such refinements will be largely masked by *noise* in a real system, as shown by Merkowitz and Johnson [50], and this must therefore be considered first. So the next step is to include noise in the model and see its effect. Stevenson [58] has already made some progress in this direction, and partly assessed the characteristics of *TIGA* and *PHC*, but more needs to be done since not too high signal-to-noise ratios should realistically be be considered in an actual GW detector. In particular, *mode channels* are at the basis of noise correlations and dependencies, as well as the errors in GW parameter estimation [51]. I do expect the analytic tools developed in this article to provide a powerful framework to address the fundamental problems of *noise* in a spherical GW antenna which, to my knowledge, have not yet received the detailed attention they require.

Acknowledgments

I am greatly indebted with Stephen Merkowitz both for his kind supply of the *TIGA* prototype data, and for continued encouragement and illuminating discussions. I am also indebted with Curt Cutler for addressing my attention to an initial error in the general equations of section 2, and with Eugenio Coccia for many discussions. M.A. Serrano gave me valuable help in some of the calculations of Appendix A.2

below, and this is gratefully acknowledged, too. I have received financial support from the Spanish Ministry of Education through contract number PB96-0384, and from Institut d'Estudis Catalans.

Appendices

A.1 Green functions for the multiple resonator system

The density of forces in he rhs of equation (82.a) happens to be of the *separable* type

$$\mathbf{f}(\mathbf{x},t) = \sum_{\alpha} \mathbf{f}^{(\alpha)}(\mathbf{x})\, g^{(\alpha)}(t) \tag{145}$$

where α is a suitable label. It is recalled from reference [37] that, in such circumstances, a formal solution can be written down for equation (82.a) in terms of a *Green function integral*, whereby the following orthogonal series expansion obtains:

$$\mathbf{u}(\mathbf{x},t) = \sum_{\alpha} \sum_{N} \omega_N^{-1}\, f_N^{(\alpha)}\, \mathbf{u}_N(\mathbf{x})\, g_N^{(\alpha)}(t) \tag{146}$$

where

$$f_N^{(\alpha)} \;\equiv\; \frac{1}{\mathcal{M}} \int_{\text{Sphere}} \mathbf{u}_N^*(\mathbf{x}) \cdot \mathbf{f}^{(\alpha)}(\mathbf{x})\, d^3x \tag{147.a}$$

$$g_N^{(\alpha)}(t) \;\equiv\; \int_0^t g^{(\alpha)}(t')\, \sin\omega_N(t-t')\, dt' \tag{147.b}$$

Here, ω_N and $\mathbf{u}_N(\mathbf{x})$ are the eigenfrequencies and associated normalised wave-functions of the free sphere. Also, N is an abbreviation for a multiple index $\{nlm\}$. The generic index α is a label for the different pieces of interaction happening in the system. I quote the result of the calculations of the terms needed in this paper:

$$f^{(a)}_{\text{resonators},N} \;=\; \frac{M_a}{\mathcal{M}}\, \Omega_a^2\, \left[\mathbf{n}_a \cdot \mathbf{u}_N^*(\mathbf{x}_a)\right] \;, \qquad a = 1,\ldots,J \tag{148.a}$$

$$f^{(l'm')}_{\text{GW},N} \;=\; a_{nl}\, \delta_{ll'}\, \delta_{mm'} \;, \qquad N \equiv \{nlm\} \;,\;\; l' = 0, 2 \;,\;\; m' = -l', \ldots, l' \tag{148.b}$$

$$f_{\text{stroke},N} \;=\; \mathcal{M}^{-1}\, \mathbf{f}_0 \cdot \mathbf{u}_N^*(\mathbf{x}_0) \tag{148.c}$$

where the coefficients a_{nl} in (148.b) are overlapping integrals of the type (147.a), and

$$g^{(a)}_{\text{resonators},N}(t) \;=\; \int_0^t \left[z_a(t') - u_a(t)\right] \sin\omega_N(t-t')\, dt' \;, \qquad a = 1,\ldots,J \tag{149.a}$$

$$g^{(lm)}_{\text{GW},N}(t) \;=\; \int_0^t g^{(lm)}(t')\, \sin\omega_N(t-t')\, dt' \tag{149.b}$$

$$g_{\text{stroke},N}(t) \;=\; \sin\omega_N t \tag{149.c}$$

If this is replaced into (82.a) one readily finds

$$\mathbf{u}(\mathbf{x},t) = \sum_{N} \omega_N^{-1}\, \mathbf{u}_N(\mathbf{x}) \left\{ \sum_{b=1}^{J} \frac{M_b}{\mathcal{M}}\, \Omega_b^2\, \left[\mathbf{n}_b \cdot \mathbf{u}_N^*(\mathbf{x}_b)\right] g^{(b)}_{\text{resonators},N}(t) + \sum_{\alpha} f^{(\alpha)}_{\text{external},N}\, g^{(\alpha)}_{\text{external},N}(t) \right\} \tag{150}$$

where the label "external" explicitly refers to agents acting upon the system from outside. Two kinds of such external actions are considered in this article: those due to GWs and those due to a calibration hammer stroke signal. Specifying $\mathbf{x}=\mathbf{x}_a$ in the lhs of (150) and multiply on either side by $\mathbf{n}_a$, the following is readily found:

$$u_a(t) = u_a^{\text{external}}(t) + \sum_{b=1}^{J} \eta_b \int_0^t K_{ab}(t-t')\ [\, z_b(t') - u_b(t')]\ dt' \tag{151.a}$$

$$\ddot{z}_a(t) = \xi_a^{\text{external}}(t) - \Omega_a^2\ [\, z_a(t) - u_a(t)]\ , \qquad a=1,\ldots,J \tag{151.b}$$

where $\eta_b \equiv M_b/\mathcal{M}$, $u_a^{\text{external}}(t) \equiv\ \mathbf{n}_a\cdot\mathbf{u}^{\text{external}}(\mathbf{x}_a,t)$,

$$\mathbf{u}^{\text{external}}(\mathbf{x},t) = \sum_{\alpha}\sum_{N} \omega_N^{-1}\, f^{(\alpha)}_{\text{external},N}\, \mathbf{u}_N(\mathbf{x})\, g^{(\alpha)}_{\text{external},N}(t) \tag{152}$$

and

$$K_{ab}(t) \equiv \Omega_b^2 \sum_{N} \omega_N^{-1}\ [\mathbf{n}_b\cdot\mathbf{u}_N^*(\mathbf{x}_b)]\,[\mathbf{n}_a\cdot\mathbf{u}_N(\mathbf{x}_a)]\,\sin\omega_N t \tag{153}$$

The following bare sphere responses to GWs and hammer strokes (equations!(81) and (89), respectively) can be calculated by direct substitution. The results as best presented as Laplace transform domain functions:

$$\hat{u}_a^{\text{GW}}(s) = \sum_{\substack{l=0 \text{ and } 2\\ m=-l,\ldots,l}} \left(\sum_{n=1}^{\infty} \frac{a_{nl}\, A_{nl}(R)}{s^2+\omega_{nl}^2}\right) Y_{lm}(\mathbf{n}_a)\, \hat{g}^{(lm)}(s)\ , \qquad a=1,\ldots,J \tag{154.a}$$

$$\hat{u}_a^{\text{stroke}}(s) = -\sum_{nl} \frac{f_0}{s^2+\omega_{nl}^2}\ |A_{nl}(R)|^2\ P_l(\mathbf{n}_a\cdot\mathbf{n}_0)\ , \qquad a=1,\ldots,J \tag{154.b}$$

where Y_{lm} are spherical harmonics and P_l Legendre polynomials [21]. The calculation of the Laplace transform of the kernel matrix (153) is likewise immediate:

$$\hat{K}_{ab}(s) = \sum_{N} \frac{\Omega_b^2}{s^2+\omega_N^2}\ [\mathbf{n}_b\cdot\mathbf{u}_N^*(\mathbf{x}_b)]\,[\mathbf{n}_a\cdot\mathbf{u}_N(\mathbf{x}_a)] \tag{155}$$

Given that (see [37] for full details)

$$\mathbf{u}_{nlm}(\mathbf{x}) = A_{nl}(r)\, Y_{lm}(\theta,\varphi)\,\mathbf{n} - B_{nl}(r)\, i\mathbf{n}\times\mathbf{L}Y_{lm}(\theta,\varphi) \tag{156}$$

and that the spheroidal frequencies ω_{nl} are $2l{+}1$–fold degenerate, (155) can be easily summed over the degeneracy index m, to obtain

$$\hat{K}_{ab}(s) = \sum_{nl} \frac{\Omega_b^2}{s^2+\omega_{nl}^2}\ |A_{nl}(R)|^2\ \left[\sum_{m=-l}^{l} Y_{lm}^*(\mathbf{n}_b)\, Y_{lm}(\mathbf{n}_a)\right] \tag{157}$$

or, equivalently,

$$\hat{K}_{ab}(s) = \sum_{nl} \frac{\Omega_b^2}{s^2+\omega_{nl}^2}\ |A_{nl}(R)|^2\ \frac{2l+1}{4\pi}\, P_l(\mathbf{n}_a\cdot\mathbf{n}_b) \tag{158}$$

where use has been made of the summation formula for the spherical harmonics [21]

$$\sum_{m=-l}^{l} Y^*_{lm}(\mathbf{n}_b)\, Y_{lm}(\mathbf{n}_a) = \frac{2l+1}{4\pi}\, P_l(\mathbf{n}_a \cdot \mathbf{n}_b) \tag{159}$$

and where P_l is a Legendre polynomial:

$$P_l(z) = \frac{1}{2^l\, l!}\, \frac{d^l}{dz^l}\, (z^2-1)^l \tag{160}$$

A.2 System response algebra

From equation (103), i.e.,

$$\sum_{b=1}^{J} \left[\delta_{ab} + \eta \sum_{nl} \frac{\Omega^2 s^2}{(s^2+\Omega^2)(s^2+\omega_{nl}^2)}\, \chi_{ab}^{(nl)} \right] \hat{q}_b(s) = -\frac{s^2}{s^2+\Omega^2}\, \hat{u}_a^{\mathrm{GW}}(s) + \frac{\hat{\xi}_a^{\mathrm{GW}}(s)}{s^2+\Omega^2}\ , \qquad (\Omega = \omega_{n_0 l_0}) \tag{161}$$

we must first isolate $\hat{q}_b(s)$, then find inverse Laplace transforms to revert to time domain quantities. Substituting the values of $\hat{u}_a^{\mathrm{GW}}(s)$ and $\hat{\xi}_a^{\mathrm{GW}}(s)$ from (154.a) and (104) into (161) we find

$$\hat{q}_a(s) = \sum_{\substack{l\,=\,0 \text{ and } 2 \\ m\,=\,-l,\ldots,l}} \hat{\Phi}_a^{(lm)}(s)\, \hat{g}^{(lm)}(s)\ , \qquad a = 1, \ldots, J \tag{162}$$

where

$$\hat{\Phi}_a^{(lm)}(s) = -\frac{s^2}{s^2+\Omega^2} \left(-\frac{R}{s^2} + \sum_{n=1}^{\infty} \frac{a_{nl}\, A_{nl}(R)}{s^2+\omega_{nl}^2} \right) \sum_{b=1}^{J} \left[\delta_{ab} + \eta \sum_{nl} \frac{\Omega^2 s^2}{(s^2+\Omega^2)(s^2+\omega_{nl})^2}\, \chi_{ab}^{(nl)} \right]^{-1} Y_{lm}(\mathbf{n}_b) \tag{163}$$

Now, using the convolution theorem of Laplace transforms, we see that the time domain version of equation (162) is

$$q_a(t) = \sum_{lm} \int_0^t \Phi_a^{(lm)}(t-t')\, g^{(lm)}(t')\, dt'\ , \qquad a = 1, \ldots, J \tag{164}$$

where $\Phi_a^{(lm)}(t)$ is the *inverse Laplace transform* of (163). The inverse Laplace transform of $\hat{\Phi}_a^{(lm)}(s)$ can be expediently calculated by the *residue theorem* through the formula [26]

$$\Phi_a^{(lm)}(t) = 2\pi i \sum \left\{ \text{residues of } \left[\hat{\Phi}_a^{(lm)}(s)\, e^{st} \right] \text{ at its poles in complex } s-\text{plane} \right\} \tag{165}$$

Clearly thus, the *poles* of $\hat{\Phi}_a^{(lm)}(s)$ must be determined in the first place. It is immediately clear from equation (163) that there are no poles at either $s=0$, or $s=\pm i\Omega$, or $s=\pm i\omega_{nl}$, for there are exactly compensated infinities at these locations. The only possible poles lie at those values of s for which the matrix in square brackets in (163) is not invertible, and these of course correspond to the zeroes of its determinant, i.e.,

$$\Delta(s) \equiv \det \left[\delta_{ab} + \eta\, \frac{s^2}{s^2+\Omega^2}\, \hat{K}_{ab}(s) \right] = 0\ , \qquad \text{poles} \tag{166}$$

There are infinitely many roots for equation (166), but *analytic* expressions cannot be found for them. *Perturbative* approximations in terms of the small parameter η will thus be applied instead. It is assumed that

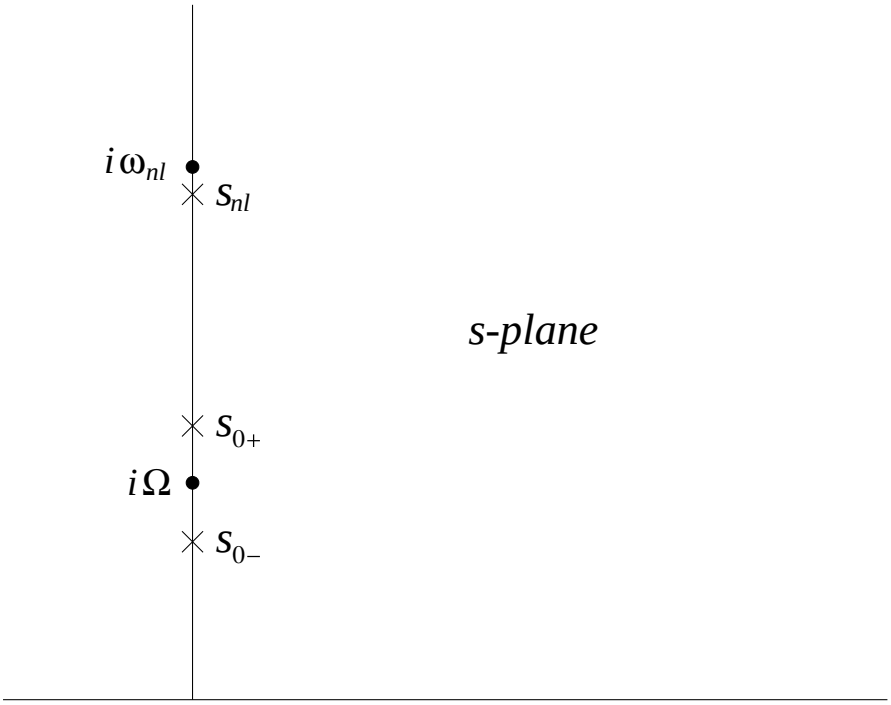

Figure 7: Position of the roots (169) in the complex s–plane for Ω tuned to the lowest frequency of the sphere's spectrum. Note that s_{nl} is closer to $i\omega_{nl}$ than $s_{0\pm}$ are to $i\Omega$; this is a consequence of the differences being proportional to η and $\eta^{1/2}$, respectively, as seen in equations (169).

$$\Omega = \omega_{n_0 l_0} \tag{167}$$

for a *fixed* multipole harmonic $\{n_0 l_0\}$. Equation (166) can then be recast in the more convenient form

$$\Delta(s) \equiv \det\left[\delta_{ab} + \eta\,\frac{\Omega^2 s^2}{(s^2+\Omega^2)^2}\,\chi_{ab}^{(n_0 l_0)} + \eta \sum_{nl\neq n_0 l_0} \frac{\Omega^2 s^2}{(s^2+\Omega^2)(s^2+\omega_{nl}^2)}\,\chi_{ab}^{(nl)}\right] = 0 \tag{168}$$

Since η is a small parameter, the *denominators* of the fractions in the different terms in square brackets in (168) must be *quantities of order* η at the root locations for the determinant to vanish at them. A distinction however arises depending on whether s^2 is close to $-\Omega^2$ or to the other $-\omega_{nl}^2$. There are accordingly two categories of roots, more precisely:

$$s_0^2 = -\Omega^2\left(1 + \chi_{\frac{1}{2}}\,\eta^{1/2} + \chi_1\,\eta + \ldots\right) \qquad (\Omega = \omega_{n_0 l_0}) \tag{169.a}$$

$$s_{nl}^2 = -\omega_{nl}^2\left(1 + b_1^{(nl)}\,\eta + b_2^{(nl)}\,\eta^2 + \ldots\right) \qquad (nl \neq n_0 l_0) \tag{169.b}$$

Figure 7 provides a visual characterisation of these roots. The coefficients $\chi_{\frac{1}{2}}$, χ_1,... and $b_1^{(nl)}$, $b_1^{(nl)}$,... can be calculated recursively, starting form the first, by substitution of the corresponding series expansions into equation (168). The lowest order terms are easily seen to be given by

$$\det\left[\delta_{ab} - \frac{1}{\chi_{\frac{1}{2}}^2}\,\chi_{ab}^{(n_0 l_0)}\right] = 0 \tag{170}$$

and

$$\det\left[\frac{\Omega^2-\omega_{nl}^2}{\omega_{nl}^2}\,b_1^{(nl)}\,\delta_{ab}-\chi_{ab}^{(nl)}\right]=0 \tag{171}$$

respectively. Both equations (170) and (171) are algebraic eigenvalue equations. As shown in appendix A.3, the matrix $\chi_{ab}^{(nl)}$ has at most $(2l+1)$ non-null positive eigenvalues —all the rest up to J are identically zero.

As a final step we must evaluate (165). This is accomplished by standard textbook techniques (see e.g. [55]); the algebra is quite straightforward but rather lengthy, and I shall not delve into its details here, but quote only the most interesting results. It appears that the *dominant* contribution to $\Phi_a^{(lm)}(t)$ comes from the poles at the locations (169.a), whereas all other poles only contribute as higher order corrections; generically, $\Phi_a^{(lm)}(t)$ is seen to have the form

$$\Phi_a^{(lm)}(t)\propto\eta^{-1/2}\sum_{\zeta_c\neq 0}\left(\sin\omega_{c+}t-\sin\omega_{c-}t\right)\,\delta_{ll_0}+O(0) \tag{172}$$

where

$$\omega_{a\pm}^2=\Omega^2\left(1\pm\sqrt{\frac{2l+1}{4\pi}}\,|A_{n_0l_0}(R)|\,\zeta_a\,\eta^{1/2}\right)+O(\eta)\;,\qquad a=1,\ldots,J \tag{173}$$

In Laplace domain one has,

$$\hat\Phi_a^{(lm)}(s)\propto\eta^{-1/2}\sum_{\zeta_c\neq 0}\left[\left(s^2+\omega_{c+}^2\right)^{-1}-\left(s^2+\omega_{c-}^2\right)^{-1}\right]\,\delta_{ll_0} \tag{174}$$

Detailed calculation of the residues [57] yield equation (106), which must be evaluated for each particular tuning and resonator distribution, as described in section 4.

A.3 Eigenvalue properties

This Appendix presents a few important properties of the matrix $P_l(\mathbf{n}_a\cdot\mathbf{n}_b)$ for arbitrary l and resonator locations $\mathbf{n}_a$ (a=1,...,J) which are useful for detailed system resonance characterisation.

Recall the *summation formula* for spherical harmonics [21]:

$$\sum_{m=-l}^{l}Y_{lm}^*(\mathbf{n}_a)\,Y_{lm}(\mathbf{n}_b)=\frac{2l+1}{4\pi}\,P_l(\mathbf{n}_a\cdot\mathbf{n}_b)\;,\qquad a,b=1,\ldots,J \tag{175}$$

where P_l is a Legendre polynomial

$$P_l(z)=\frac{1}{2^l\,l!}\,\frac{d^l}{dz^l}\,(z^2-1)^l \tag{176}$$

To ease the notation I shall use the symbol $\mathcal{P}_l$ to mean the entire $J\times J$ matrix $P_l(\mathbf{n}_a\cdot\mathbf{n}_b)$, and introduce Dirac *kets* $|m\rangle$ for the column J-vectors

$$|m\rangle\equiv\sqrt{\frac{4\pi}{2l+1}}\begin{pmatrix}Y_{lm}(\mathbf{n}_1)\\ \vdots\\ Y_{lm}(\mathbf{n}_J)\end{pmatrix}\;,\qquad m=-l,\ldots,l \tag{177}$$

These kets are *not* normalised; in terms of them equation (175) can be rewritten in the more compact form

$$\mathcal{P}_l = \sum_{m=-l}^{l} |m\rangle\langle m| \tag{178}$$

Equation (178) indicates that the *rank* of the matrix $\mathcal{P}_l$ cannot exceed $(2l+1)$, as there are only $(2l+1)$ kets $|m\rangle$. So, if $J > (2l+1)$ then it has at least $(J-2l-1)$ identically null eigenvalues —there can be more if some of the $\mathbf{n}_a$'s are parallel, as this causes rows (or columns) of $\mathcal{P}_l$ to be repeated.

We now prove that the non-null eigenvalues of $\mathcal{P}_l$ are *positive*. Clearly, a regular eigenvector, $|\phi\rangle$, say, of $\mathcal{P}_l$ will be a linear combination of the kets $|m\rangle$:

$$\mathcal{P}_l\,|\phi\rangle = \zeta^2\,|\phi\rangle\ , \qquad |\phi\rangle = \sum_{m=-l}^{l} \phi_m\,|m\rangle \tag{179}$$

where ζ^2 is the corresponding eigenvalue, having a positive value, as we now prove. If the second (179) is substituted into the first then it is immediately seen that

$$\sum_{m'=-l}^{l} \Big(\zeta^2\,\delta_{mm'} - \langle m|m'\rangle\Big)\ \phi_{m'} = 0 \tag{180}$$

which admits non-trivial solutions if and only if

$$\det\ \Big(\zeta^2\,\delta_{mm'} - \langle m|m'\rangle\Big) = 0 \tag{181}$$

In other words, ζ^2 are the eigenvalues of the $(2l+1)\times(2l+1)$ matrix $\langle m|m'\rangle$, which is positive definite because so is the "scalar product" $\langle\phi|\phi'\rangle$. All of them are therefore strictly positive.

Finally, since the *trace* is an invariant property of a matrix, and

$$\mathrm{trace}(\mathcal{P}_l) \equiv \sum_{a=1}^{J} P_l(\mathbf{n}_a\cdot\mathbf{n}_a) = \sum_{a=1}^{J} 1 = J \tag{182}$$

we see that the eigenvalues ζ_a^2 add up to J:

$$\mathrm{trace}(\mathcal{P}_l) = \sum_{a=1}^{J} \zeta_a^2 \equiv \sum_{\zeta_a\neq 0} \zeta_a^2 = J \tag{183}$$

References

[1] Abramowitz M. and Stegun I.A., *Handbook of Mathematical Functions*, Dover 1972.

[2] Ashby N. and Dreitlein J., *Phys. Rev.* **D12**, 336 (1975).

[3] Astone P. *et al.*, *Europhys. Lett.* **16**, 231 (1991).

[4] Astone P. *et al*, *Phys. Rev.* **D47**, 2 (1993).

[5] Astone P., Lobo J.A. and Schutz B.F., *Class Quan Grav* **11**, 2093 (1994).

[6] Astone P. et al., "*SFERA*: Proposal for a spherical GW detector", Roma 1997.

[7] Barut A.O., *Electrodynamics and Classical Theory of Fields and Particles*, Dover 1980.

[8] Bassan M., Cosmelli C., Frasca S., Papa M.A., Puppo P., Rapagnani P. and Ricci F., *High Frequency Gravitational Array*, "La Sapienza" preprint, Roma 1994.

[9] Bianchi M., Coccia E, Colacino C. N., Fafone V., Fucito F., *Class Quan Grav* **13**, 2865 (1996).

[10] Bianchi M., Brunetti M., Coccia E., Fucito F, Lobo J. A., *Phys. Rev.* **D57**, 4525 (1998).

[11] Brans C. and Dicke R. H., *Phys. Rev.* **124**, 925 (1961)

[12] Eugenio Coccia, personal communication.

[13] Coccia E., Lobo J.A. and Ortega J.A., *Phys. Rev.* **D52**, 3735 (1995).

[14] Coccia E., Pizzella G., Ronga F., eds., Proceedings of the First Edoardo Amaldi Conference, World Scientific, Singapore 1995.

[15] Coccia E. and Fafone V., *Phys Lett A* **213**, 16 (1996).

[16] Coccia E., in Francaviglia M., Longhi G., Lusanna L., and Sorace E., eds., Proceedings of the GR-14 Conference, World Scientific, Singapore 1997.

[17] Coccia E., Fafone V., Frossati G., Lobo J. A. and Ortega J. A., *Phys. Rev.* **D57**, 2051 (1998).

[18] Dhurandhar S. V., Krolak A., Lobo J. A., *Mon Not of Roy Ast Soc*, **237**, 333 (1989), and **238**, 1407 (1989).

[19] Dhurandhar S. V. and Tinto M., *Mon Not of the Royal Ast Soc*, **236**, 621 (1989).

[20] Eardley D.M., Lee D.L. and Lightman A.P., *Phys Rev* **D8**, 3308 (1973).

[21] Edmonds A.R., *Angular Momentum in Quantum Mechanics*, Princeton Univ. Press 1960.

[22] Forward R., *Gen Rel and Grav* **2**, 149 (1971).

[23] See e.g. Hamilton O.W. in Gleiser R.J., Kozameh C.N. and Moreschi O.M., *Proceedings of GR13, Córdoba, Argentina*, IOP 1993. Also, Hamilton O.W. in reference [14] above.

[24] Hamilton W. O., Johnson W. W., Xu B. X., Solomonson N., Aguiar O. D., *Phys Rev* **D40**, 1741 (1989).

[25] Har'El Z., *Geometriæ Dedicata* **47**, 57 (1993).

[26] Helstrom C.W., *Statistical Theory of Signal Detection*, Pergamon Press 1968.

[27] Hier R.G. and Rasband S.N., *Ap Jour* **195**, 507 (1975).

[28] Holden A., *Formes, espace et symétries*, CEDIC, Paris 1977.

[29] Warren Johnson, private communication during the First Edoardo Amaldi Meeting in Frascati, June 1994.

[30] Johnson W. and Merkowitz S. M.,*Phys. Rev. Lett.* **70**, 2367 (1993).

[31] Krolak A., Lobo J. A., Meers B. J., *Phys Rev* **D43**, 2470 (1991).

[32] Landau L.D. and Lifshitz E.M., *Theory of Elasticity*, Pergamon Press 1970.

[33] Landau L.D. and Lifshitz E.M., *The Classical Theory of Fields*, Pergamon Press 1985.

[34] Lobo J.A. and Ortega J.A., in Coccia E., Pizzella G., Ronga F., eds., *Proceedings of the First Edoardo Amaldi Conference on Gravitational Waves* (Frascati 1994), pag 449, World Scientific, Singapore (1995).

[35] I take this denomination from reference [53]. It is, apparently, less common in the classical literature than the term *toroidal* applied to the other modes.

[36] Lobo J.A., unpublished.

[37] Lobo J. A., *Phys Rev* **D52**, 591 (1995). This paper constitutes the first part of the present file, *What can we learn about GW Physics with an elastic spherical antenna?*.

[38] Lobo J. A. and Serrano M. A., Europhys Lett, **35**, 253 (1996).

[39] Lobo J.A., in A. Królak, ed, *Mathematics of Gravitation*, Banach Center Publications, vol 41, part II, pag 163-178, Warszawa (1997).

[40] Lobo J. A. and Serrano M. A., *Class Quan Grav* **14**, 1495 (1997).

[41] Lobo J.A., in E. Coccia, G. Pizzella, G. Veneziano, eds, *Proceedings of the Second Edoardo Amaldi Conference on Gravitational Waves* (*CERN*, Geneva 1997), pag 168-179, World Scientific Singapore (1998).

[42] Love A.E.H., *A Treatise on the Mathematical Theory of Elasticity*, Dover 1944.

[43] Magalhães N. S., Johnson W.W., Frajuca C, Aguiar O., *Mon Not of the Royal Ast Soc*, **274**, 670 (1995).

[44] Magalhães N. S., Aguiar O. D., Johnson W. W., Frajuca C., *Gen Rel and Grav* 29, 1509 (1997).

[45] Merkowitz S. M., PhD Thesis Memoir, Louisiana State University (1995).

[46] Merkowitz S. M. and Johnson W. W., *Phys Rev* **D51**, 2546 (1995).

[47] Merkowitz S. M. and Johnson W. W., *Phys Rev* **D53**, 5377 (1996).

[48] Merkowitz S. M. and Johnson W. W., *Phys Rev* **D56**, 7513 (1997).

[49] Merkowitz S. M., *Phys Rev* **D58**, 062002 (1998).

[50] Merkowitz S. M. and Johnson W. W., *Europhys Lett*, **41**, 355 (1998).

[51] Merkowitz S. M., Lobo J. A., Serrano M. A., *Class Quan Grav* **16**, 3035 (1999).

[52] Merkowitz S. M., Coccia E., Fafone V., Raffone G., Schipilliti M., and Visco M., *Rev Sci Instr*, **70**, 1553 (1999).

[53] Michelson P.F. and Zhou C.Z., *Phys. Rev.* **D51**, 2517 (1995).

[54] Misner, Thorne, Wheeler, *Gravitation*, Freeman 1973.

[55] Porter D. and Stirling D. S. G., 1990, Integral equations: a practical treatment from spectral theory to applications, Cambridge University Press

[56] Rasband S.N., *J Acous Soc Am* **57**, 899 (1975).

[57] Serrano M. A., PhD Thesis, University of Barcelona (1999).

[58] Stevenson T. R., *Phys. Rev.* **D56**, 564 (1997).

[59] Tricomi F. G., *Integral equations*, Interscience Publishers 1957.

[60] Tym Myint–U, *Partial Differential Equations for Scientists and Engineers*, North Holland 1987.

[61] Wagoner R. V. and Paik H. J. in *Experimental Gravitation*, Proceedings of the Pavia International Symposium, Acad. Naz. dei Lincei 1977.

[62] Weinberg S., *Gravitation and Cosmology*, Wiley 1972.